Downregulation of Perilipin1 by IMD leads to LD reconfiguration and adaptation to bacterial infection in *Drosophila*

Lei Wang[1,2,5*], Jiaxin Lin[2,3,5*], Junjing Yu[4], Kaiyan Yang[2,3,5], Li Sun[2,3,5], Hong Tang[2 #] and Lei Pan[2,3,6 #]

[1] Wuhan Institute of Virology, Chinese Academy of Sciences, Wuhan, Hubei 430071, China

[2] The Center for Microbes, Development and Health; Key Laboratory of Molecular Virology and Immunology, Institut Pasteur of Shanghai, Chinese Academy of Sciences, Shanghai 200031, China

[3] CAS Center for Excellence in Biotic Interactions, University of Chinese Academy of Sciences, Beijing 100049, China

[4] Shanghai Institute of Biochemistry and Cell Biology, Chinese Academy of Sciences, Shanghai 200031, China.

[5] University of Chinese Academy of Sciences, Beijing 100049, China

[6] Lead contact

* These authors contribute equally.

#Correspondence: H. Tang (htang@ips.ac.cn) or L. Pan (panlei@ips.ac.cn).

ABSTRACT

Lipid droplets（LDs）are dynamic intracellular organelles critical for lipid metabolism. Dynamic alterations in the configurations and functions of LDs during innate immune response to bacterial infections and the underlying mechanisms however, remain largely unknown. Herein, we trace the time-course morphology of LDs in fat bodies of *Drosophila* after transient bacterial infection. Detailed analysis shows that *perilipin1* (*plin1*), a core gene regulating lipid metabolism of LDs is suppressed by IMD/Relish, an innate immune signaling. During immune activation, downregulated *plin1* promotes the enlargement of LDs, which in turn alleviates immune reaction-associated reactive oxygen species (ROS) stress. Thus, the growth of LDs is likely an active adaptation to maintain redox homeostasis in response to IMD activation. Therefore, our study provides evidence that *plin1* serves as a modulator on LDs' reconfiguration in regulating infection-induced pathogenesis, and Plin1 might be a potential therapeutic target for coordinating inflammation resolution and lipid metabolism.

INTRODUCTION

Immune activation is essentially accompanied by metabolic reprogramming, which redistributes accessible energy to prioritize immune protection against pathogenic infections (1, 2). Thus, stringent regulation of metabolic machinery in response to immunoreaction is critical for the host fitness. Besides carbohydrates, lipids provide another important bioenergetic and synthetic resource to the host. Not limit to this, a number of lipid metabolites in turn have been reported to play key roles in pro- or anti-inflammatory pathways (3-5). In all eukaryotic and some prokaryotic cells, there are

46 important intracellular organelles, lipid droplets (LDs), which provide a major place for
47 the synthesis, lysis, transfer and storage of lipids or their derived metabolites (6). LDs
48 contain a hydrophobic core of neutral lipids, such as di/triacylglycerols or sterol esters,
49 which is surrounded with a phospholipid monolayer decorated by different proteins (7).
50 Previously, LDs were considered to get involved in many physiological and
51 pathological processes just because of their main functions on storing/providing energy
52 and/or buffering toxic lipid species through modulating enzymic or autophagic lipolysis
53 (8, 9). So far, emerging evidences have shown that LDs also take part in immune
54 regulation. For instance, LDs modulate functions of myeloid cell through immune-
55 metabolic reprogramming (10). LDs facilitate hosts to combat pathogens' infections
56 through selectively recruiting immune proteins (11, 12). Recently, a study indicated that
57 mammalian LDs respond to bacterial lipopolysaccharide and function as innate immune
58 hubs to coordinate host defense and cell metabolism (13). However, the role of LDs as
59 pro- or anti-inflammatory modulators is still controversial (14), due to fact that LDs are
60 highly dynamic organelles. The number, size and anchored proteins of LDs change
61 quickly in response to infection or stress (15-17). These evidences also indicate that the
62 status of LDs should be tightly controlled. Defects in the biogenesis and mobilization
63 of LDs not only result in lipotoxicity (18, 19) but also exacerbate inflammatory
64 responses and organelles dysfunction (20, 21). However, the role and dynamic pattern
65 of LDs during immune process is still barely described. Especially, the factors
66 mediating the transformation of LDs underlying immunometabolic switches have not
67 been well identified.

68

69 LDs are non-homogenous organelles, which accommodates hundreds of variable
70 proteins (22, 23). However, Perilipins (Plins) are the most prominent proteins that span
71 the surface of LDs (24, 25). Each LD is usually decorated by two or more members of
72 Perilipin family proteins and no LDs without perilipins have been identified in
73 mammalian cells so far (26). There are five major perilipins in mammalian, named
74 Perilipin1-5. These Perilipins differ in the expression and cellular localization in
75 different tissues and have essential roles in the regulation of LDs' structure and
76 morphology (27, 28). However, whether Perilipins get involved in immune functions,
77 probably through mediating LDs' reconfiguration, is still obscure. In human or mouse
78 adipocyte tissue, Perilipin1 deficiency leads to uncontrollable LDs lipolysis and
79 infiltration of inflammatory cells (29, 30). Inhibition of lipases, such as adipose
80 triglyceride lipase (ATGL) or hormone-sensitive lipase (HSL), can alleviate this
81 metaflammation (31, 32). *Plin1* knockout also promotes secretion of prostaglandins,
82 the pro-inflammatory lipid metabolites, and elevates pro-inflammatory M1-type
83 adipose tissue microphages in mice (33). In innate immunity, the expression and
84 localization of Perilipins on LDs changed in response to LPS stimulation, which
85 subsequently affected antimicrobial capacity (13). These evidences suggest a link
86 between Perilipins and immunometabolic regulations.

87

88 *Drosophila melanogaster* has emerged as a productive organism to investigate
89 immunometabolism, due to the advantages of powerful genetic manipulation and

90 highly conserved mechanisms in both innate immunity and metabolism (34-36).
91 Especially, the fat body (analogous to human liver and adipose tissue), as a major organ
92 mediating systemic innate immunity, is an ideal place for studying the interaction
93 between metabolism and inflammation of LDs, due to its richness in LDs (37, 38).
94 Furthermore, Perilipins are evolutionarily conserved from fungi to human. Not like
95 more redundant Plins in mammalian, there are only two Plins in *Drosophila*, Lipid
96 storage droplet-1 (*lsd1* or *plin1*) and *lsd2* (*plin2*) (39). Plin2 acts to promote lipid storage
97 and LDs' growth as a barrier for lipase (40-42), while Plin1 modulates protein flux on
98 LDs (27, 28). They have opposite functions on the control of LDs' morphology (27). In
99 *Drosophila*, the immune deficiency (IMD) pathway is a dominant innate immune
100 singling against Gram-negative bacterial infections, which is homologue to mammalian
101 NF-kB/TNF pathway (35). Couple studies have revealed that IMD signaling modulate
102 lipolysis in either fat body or intestine of flies (43, 44). And thus, LDs' accumulation
103 was once reported in fly gut after IMD activation (17). However, as if LDs adapt to
104 immune response, whether and how morphological changes occur on LDs remain
105 unclear. More importantly, the contribution of theses adaptive altered LDs to infectious
106 pathogenesis and the underlying mechanisms mediating by LDs-anchored factors such
107 as Plins, are still poorly understood.
108
109 In this study, the alteration in morphology and number of LDs were traced dynamically
110 during bacterial infection. Plin1 was found to respond to IMD action and then modify
111 LDs' morphology to alleviate inflammatory stress. Our data reveal that adaptive

112 modification of LDs acts as an active modulator of infection-induced pathogenesis.

113

114 **Results**

115 **Bacterial infection modulates lipid metabolism, and particularly alters**

116 **morphology of lipid droplets (LDs) in the fat body**.

117 In *Drosophila*, the fat body is not only a central organ mediating systemic immune

118 responses, but also the epicenter for lipid metabolism. Thus, to decipher the mechanistic

119 connections between innate immunity and lipid metabolism, the kinetics of fat content

120 was tested in the fat body of *Drosophila* after systemic infection. *Escherichia. Coli* (*E.*

121 *coli*), a non-pathogenic Gram-negative bacterium to flies, was used to perform nano-

122 injection to infect adult male fruit flies. The immune deficiency (IMD) pathway is a

123 dominant innate immune signaling against Gram-negative bacterial infections that

124 regulates Relish/NF-κB-dependent transcription of AMPs, such as *Diptericin* (*Dpt*)

125 (35). Thus, by measuring the expression level of *Dpt,* IMD signaling activity could be

126 monitored (45, 46). In consistent with previous report that *E.coli* injection resulted in a

127 transient innate immune response within 48 hour post infection (hpi)(47), a gradient

128 increase in IMD activity in the fat body was observed from 0 hpi to 12 hpi, and then

129 this activity subsided to the basal level after 48 hpi (**Fig.1A**). Interestingly, compared

130 to mock injection control (**Supplementary Fig. S1A**), the fat levels in the fat body of

131 flies with *E.coli* infection steadily increased from 4 hpi to 16 hpi and then almost

132 recovered after 48 hpi (**Fig. 1A**). Therefore, these results suggest a link between lipid

133 metabolism and IMD signaling activation in the fat body of flies.

134

135 LDs are the main site for lipid metabolism, mobilization and storage (48), which
136 prompted us to investigate whether LDs change in the fat body in response to bacterial
137 infection. BODIPY staining of fat body cells revealed that compared to PBS injection
138 group (**Fig. 1B and 1C**), *E. coli* infection increased the percentage of intracellular small
139 LDs (diameter < 2 μm) at 6 hpi (**Fig. 1B and 1C**). And then, LDs grew bigger at 16 hpi
140 as indicated by the decrease in the percentage of small LDs and concurrent increase in
141 the percentage of large LDs (diameter > 4 μm). Finally, this size distribution of LDs
142 was restored to basal levels at 24 hpi (**Fig. 1B and 1C**). Accordingly, the average size
143 of LDs in fat body cells had the similar changing trend (**Fig.1D**). These results indicate
144 that small LDs are prone to fuse into bigger ones during the initial 16 h after *E. coli*
145 infection.
146
147 **The reconfiguration of LDs requires IMD signaling activation.**
148 To determine whether IMD signaling activation rather than live bacterial growth is
149 responsible for the modification of LDs during infection, heat-killed *E. coli* was applied
150 to repeat infection in wild type flies. The elevated fat levels in fat bodies were still
151 observed at 12 hpi in WT flies (**Fig. 2A**). In *Drosophila*, peptidoglycan (PGN) from
152 Gram-negative bacteria can bind to the receptor of PGRP-LC to active IMD signaling
153 through transcriptional regulator Relish (35). Thus, the flies with homozygous mutation
154 of *PGRP-LC* (*PGRP-LC*$^{\Delta 5}$) or *relish* (*relish*^{E20}) was used for infection. In contrast to
155 wild type flies, the phenotype of elevated fat contents in fat bodies disappeared and
156 even reversed in these mutant flies at 12h post heat-killed *E.coli* injection (**Fig. 2B**).
157 Moreover, IMD signaling deficiency also restricted the increase in LDs size at 16 hpi,

158 compared to WT controls (**Fig. 2C and D**). Therefore, these results suggest that IMD
159 signaling activation is required to modify LDs' morphology in response to bacterial
160 infection.
161
162
163 ***plin1* is involved in LDs' morphological change induced by IMD activation.**
164 Perilipins (Plins), a group of constitutive proteins that span the surface of LDs, were
165 reported to regulate lipid mobilization and LDs' morphology (27, 28). There are two
166 Perilipins in *Drosophila*, Plin1 and Plin2. To explore whether Plins are involved in the
167 regulation of LDs' reconfiguration in response to immune activation, their time-course
168 expression was detected in the fat body by real-time PCR. *E. coli* infection induced a
169 significant downregulation of *plin1* mRNA levels at 4 hpi, which was then gradually
170 restored to basal levels at 24 hpi (**Fig.3A**). The changing trend of *plin1* expression
171 seemed to be negatively correlated with the changes in LD's size and IMD activity.
172 However, the expression level of *plin2* was only slightly tuned down at 4hpi and back
173 to normal at 12h after *E. coli* infection (**Supplementary Fig.2A**). Previous study have
174 shown that deficiency of *plin2* resulted in reduced rather than enlarged size of LDs (27).
175 Therefore, these results indicate a potential role of *plin1* in the regulation of LDs'
176 morphology in response to IMD activation. Furthermore, either deficiency of *plin1* by
177 mutation (*plin1*^{38}) or specific knockdown of *plin1* in fat body (*UAS-plin1 RNAi* driven
178 by *ppl-GAL4*) promoted the formation of large LDs. Whereas, ectopic expression of
179 *plin1* in the fat body led to the accumulation of much smaller LDs, compared with

180 controls (**Fig. 3B)**. These results were reminiscent of previous studies that Plin1 may
181 function to enhance lipid mobilization and inhibit LD coalescence (49).
182
183 Martik (MRT) /Putzig (PZG) complex, a chromosome remodeling complex, has been
184 reported to suppress *plin1* at transcriptional level (49). The mRNA levels of both *mrt*
185 and *pzg* were upregulated in the fat body after bacterial infection (**Fig. 3C and 3D**).
186 Interestingly, homologous alignment showed that at least one conserved binding motif
187 of Relish existed in the promoter region of both *mrt* and *pzg* genes across *Drosophila*
188 species with different evolutionary ages (**Supplementary Fig. S3A and S3B)**. This
189 implies a potential regulation of these genes by IMD/Relish. Peptidoglycan (PGN)
190 derived from gram-negative bacteria can activate IMD signaling in *Drosophila* S2*
191 cells *in vitro* (50). The treatment of PGN enhanced luciferase activity controlled by the
192 promoter of *mrt* or *pzg* in S2* cells, which was blocked by the knockdown of Relish
193 using dsRNA (51) (**Fig. 3E and 3F**). Additionally, two Relish binding motifs in
194 truncated *mrt* promoter region (T-*mrt(Rel)*, -870 to +1bp, in **Supplementary Fig. S3C**)
195 were required for *mrt* transcription (**Fig. 2G**), because PGN treatment didn't enhance
196 T-*mrt*-Luc activity any more when these two sites were removed (**Fig. 2G**). Thus, these
197 results suggest that suppression of *plin1* by IMD signaling might be through
198 upregulation of mrt/pzg. All together, these results provide an explanation for LDs'
199 growth in the early stages of transient IMD activation.
200
201 **Plin1 compromises host protection against bacterial infection**.

202 Naturally, whether Plin1 participated in the defense of bacterial infection was tested
203 next. Since *E. coli* is non-pathogenic to flies, another Gram-negative bacterium,
204 *Salmonella. Typhimurium* (*S. typhimurium*), which is a deadly pathogen for flies (52),
205 was used to evaluate Plin1 function on immune defense. Compared to genetic controls,
206 either *plin1* deficiency (*plin1*^{38}) (**Fig. 4A and 4B**) or fat body-specific knockdown of
207 *plin1* (*ppl-GAL4>UAS-plni1RNAi*) (**Fig. 4C and 4D**) significantly prolonged the
208 survival rate and slightly reduced bacterial loads (colony-forming units, CFUs) after *S.*
209 *typhimurium* septic infection, indicative of enhanced resistance against bacterial
210 infection. Conversely, ectopic expression of *plin1* in the fat body (*ppl-GAL4>UAS-*
211 *plin1*) led to a dramatic increase in mortality rate of flies infected with *S. typhimurium*
212 (**Fig. 4E ,** Reducing infection OD because O.E.*plin1* flies died too quickly.**)**, or even
213 by non-pathogenic *E. coli* (**Fig. 4G)**, possibly due to uncontrolled bacterial growth **(Fig.**
214 **4F and 4H**). However, it's worthy to note that deficiency of *plin1* did not affect anti-
215 microbial peptides (AMPs) (*Diptericin*, *Dpt; AttacinA, AttA*) response upon *E. coli*
216 infection (**Supplementary Fig. S4A**), but specifically improved *Dpt* expression upon
217 *S. typhimurium* infection (**Supplementary Fig. S4B**). Interestingly, overexpression of
218 *plin1* dampened AMPs response in both *E. coli* and *S. typhimurium* infections
219 (**Supplementary Fig. S4C and S4D**). Taken together, these results suggest that
220 adaptive downregulation of *plin1* in response to IMD signaling activation protected the
221 host against bacterial infections.
222
223 **Plin1-mediated reconfiguration of LDs participates in the homeostasis of**
224 **intracellular ROS.**

225 The next question is whether downregulated Plin1-induced LDs' growth also benefit
226 the host against bacterial infection. Sustained immune activation is a high energy-cost
227 process, which requires active lipolysis and usually leads to excessive reactive oxygen
228 species (ROS) accumulation due to the release and oxidation of free fatty acids, one
229 hallmark for inflammatory damages (18, 53). However, LDs' growth could efficiently
230 reduce the accumulation of free fatty acids, and probably relieve ROS-related tissue
231 damages (54). As expect, *plin1* deficiency (*plin1*^{38}) (**Fig.5A and A1**) or knockdown
232 (*UAS-plin1RNAi* driven by *ppl-GAL4*)(**Fig. 5B and B1**), which promoted LDs growth,
233 accompanied with a much lower level of ROS than that of control. In contrast,
234 overexpression of *plin1* in fat body cells（*ppl-GAL4> plin1*）, which transformed LDs
235 into smaller ones, markedly increased ROS intensity (**Fig. 5B and B1**). These results
236 suggest a correlation between the size of LDs and the intensity of ROS accumulation
237 in fat body cells. To further support this notion, we skewed ROS metabolism in fat
238 bodies through knockdown of superoxide dismutase genes (*sod1* or *sod2*) or catalase
239 gene (*cat*), all of which encode enzymes for intracellular ROS clearance (55, 56). All
240 these flies (*ppl-GAL4>UAS-sod1-RNAi*, *sod2-RNAi* or *cat-RNAi*) contained elevated
241 ROS levels (**Fig.5C and 5D**) and compensatory LD's growth in fat bodies (**Fig. 5E**
242 **and 5F**). If blocking the large LDs' formation by simultaneous overexpression of *plin1*
243 in these genetic backgrounds (**Fig. 5E and 5F**), much higher ROS accumulation was
244 observed in fat bodies (**Fig. 5C and 5D**). All together, these results suggest that Plin1-
245 controled LDs' reconfiguration takes part in antioxidative functions.
246

247 **Downregulated Plin1 in response to IMD activation benefits flies against oxidative**
248 **stress associated with bacterial infection.**

249 The activation of immune signaling, such as NF-κB or TNF signaling, often associates
250 with ROS-induced inflammatory stress (53, 57). A transgenic allele with a *gstD-GFP*
251 insertion was utilized to monitor ROS activity *in vivo* by measuring GFP intensity (58).
252 Indeed, in *Drosophila*, infection either by non-pathogenic *E.coli* or by strong
253 pathogenic *S. typhimurium* induced an obvious increase of intracellular ROS levels in
254 the fat body (**Fig. 6A and 6B**). These results support the link between bacterial infection
255 and accumulation of intracellular oxidative stress. If we removed this infection-
256 associated intracellular ROS by feeding flies with N-acetylcysteine (NAC), a widely-
257 used ROS scavenger, the survival of flies after pathogenic *S. typhimurium* infection was
258 improved, compared to non-infected controls (**Fig. 6C**). It's worthy to note that feeding
259 flies with NAC at 12 h, not 0h, post *S. typhimurium* infection, benefited the fitness of
260 flies much better. It's likely that at time point of 12 hpi, excessive ROS accumulation
261 had already developed, and initiate ROS of early infectious stage is useful for defense
262 against bacteria (59, 60). These results suggest that excessive oxidative stress, which
263 develops during bacterial infection is harmful for the host.

264

265 Since LDs are major hubs for lipid metabolism in fat body cells and function on ROS
266 clearance, it promoted us to investigate whether *plin1*-mediated LDs modification is
267 involved against bacterial infection, probably through regulating intracellular ROS. At
268 first, we found that elevated ROS levels in wild type fat bodies were diminished in fat

269 bodies of *plin1* deficiency flies (**Fig. 6D and 6E**). Next, a RU486 induced fat body-
270 specific GAL4 (*GS106-GAL4*) was used to modulate the expression of *plin1* just before
271 *S.typhimurium* infection, which exclude the possible effects of *plin1* on the
272 development of flies. As expect, overexpression or knockdown of *plin1* in the fat body
273 resulted in a significant decrease or increase in LDs' size, respectively (**Fig. 6F**).
274 Downregulation of *plin1* prolonged the survival rate after *S.typhimurium* infection (**Fig.**
275 **6G**), while ectopic expression of *plin1* shortened the life span dramatically (**Fig. 6H**).
276 Meanwhile, fluorescent probe 2',7'-dichlorofluorescein diacetate (DCFH-DA) staining
277 indicated an elevated intracellular ROS levels in *plin1*-overexpression flies and a
278 reduced ROS levels in *plin1*-knockdown flies during infection (**Fig. 6I and 6I1-2**).
279 Taken together, these results suggest that large LDs formation contributes to alleviate
280 intracellular oxidative stress induced by bacterial infection and Plin1 might serve as an
281 important modulator to promote LDs modification in response to IMD activation.
282

283 **Discussion**

284 Metabolic reprogramming of lipids has been widely reported to be associated with
285 immune responses (1, 2, 61). As a major intracellular organelle for lipid metabolism
286 and storage, LDs also seem to be involved in immune processes. Immune stimulation
287 either by infection with bacteria (62, 63), virus (64-66), fungus(67) or protozoan
288 parasites (68), or by cytokines inoculation (69, 70) may promote the biogenesis of LDs
289 in mammalian leukocytes. Recently, Hash et al also reported that LDs are infection-
290 inducible organelles in the gut of *Drosophila* at a certain timepoint after infection (17).

291 Bosch et al further indicated LDs recruit antimicrobial proteins in response to LPS and
292 function as innate immune hubs (13). However, the status and morphology of LDs
293 change rapidly *in vivo*. Whether this dynamic transformation of LDs in response to
294 immune stimulation is seldom described. Whether adaptive morphological change of
295 LDs plays active rather than passive roles in pathogenesis, and key regulators linking
296 LDs' reconfiguration and infection still need further investigated.
297
298 In this study (**Fig.7**), we carefully traced the time-course morphogenesis of LDs in the
299 fat body along with the dynamic curve of IMD signaling activity. We found that
300 transient IMD activation by bacterial infection promoted LDs' growth in the fat body
301 within 12hpi. Both LDs' size and fat levels in the fat body was maximum when IMD
302 activity almost achieved its peak. Previous studies show that transcriptional levels of
303 most triglyceride synthesis genes are suppressed during the initial phase of infection
304 (71, 72), suggesting that the substrates for LDs' biogenesis in the fat body were
305 probably imported lipids rather than *de novo* synthesized fatty acids, and IMD signaling
306 activation is required for this process. Detailed analysis showed that *plin1*
307 downregulation is critical for LDs' growth in response to transient IMD activation,
308 considering its expression was suppressed by IMD/Relish activated MRT/PZG
309 complex. Although the immune response is an energy-cost process, the fat content in
310 specific tissue such as fat body is surprisingly increasing at the early stage of immune
311 activation. These findings prompt us to imagine that LDs' biogenesis is likely an active
312 host adaptation to immune challenges. To further support this hypothesis, we found that

313 enlarged LDs benefit the host against intracellular ROS-mediated oxidative stress
314 induced by bacterial infection.
315
316 Excessive ROS accumulation is often the main cause of inflammation/infection-
317 induced cellular damages. In fact, biological processes such as cancer, neural activity,
318 and inflammation are all energy-intensive, rely on robust fat metabolism, which
319 releases large amounts of free fatty acids. The excess accumulation of free fatty acids
320 in the cytoplasm promotes lipotoxicity and ROS-induced oxidative stress (73-75). The
321 high levels of intracellular ROS can further promote lipolysis and free fatty acids
322 release (76). This vicious circle finally drives the host to enter a severe metaflammatory
323 state during chronic hyperinflammation, and consequently shorten lifespan. A recent
324 study showed that renal purge of hemolymphatic lipids can efficiently prevent ROS-
325 mediated tissue damage during inflammation (77). A similar antioxidant function of
326 LDs was also reported in neuronal stem cell niche (78) and in cancer cells (79). In our
327 study, blocking the breakdown and promoting the growth of LDs by downregulated
328 *plin1* could efficiently eliminate ROS accumulation and prolong flies' lifespan after
329 bacterial infection. However, the detailed mechanisms how large LDs prefer to prevent
330 ROS accumulation needs further investigation. One possibility is that the formation of
331 large LDs sequesters the release of excessive free lipids, which oxidation contributes to
332 the main source of ROS generation. Another possibility is that the larger the LDs are,
333 the smaller the contact areas with mitochondria are. As mitochondria provides a major
334 place for the oxidation of lipid usually supplied by LDs (9), reduced contacts between

335 LDs and mitochondria might be another not-bad way to cut down ROS generation. Thus,
336 LDs' growth is beneficial for redox homeostasis of the host. The downregulation of
337 Plin1 to promote the enlargement of LDs might be an effective host adaptation to
338 resolve inflammation-associated stress in response to immune activation.
339
340 Moreover, large LDs' formation can reduce the opportunity of pathogens to utilize free
341 fatty acids for their own growth (80-82). This is possibly one reason why *plin1* deficient
342 flies, owning bigger LDs, had lower bacterial loads after infection. In addition, larger
343 LDs might contain more resident histones, a cationic protein, which has been reported
344 to kill bacteria in a previous study (83). In mammals, IFN-γ treatment of *M. tuberculosis*
345 infected bone-marrow derived macrophage (BMDM) can induce the formation of LDs,
346 in which neutral lipids serve as a source to produce eicosanoids for enhancing host
347 defense (84). A recent study made a detailed analysis that LDs recruit cathelicidin, a
348 broad-spectrum antimicrobial peptide, in response to LPS stimulation (13). However,
349 whether the change of LDs' morphology alters the recruitment of LD-anchored proteins
350 and underlying molecular and cellular mechanisms need further investigation. In our
351 study, the reduced expression of genes encoded antimicrobial peptides was also found
352 when *plin1* overexpression (**Supplementary Fig. S4C and S4D**) and *diptericin* was
353 upregulated after *plin1* mutant flies infected with bacteria (**Supplementary Fig. S4B**).
354 These results also suggest that a link between antimicrobial signaling with *plin1* directly
355 or Plin1-mediated LDs' modification indirectly. However, the large LDs' formation in
356 response to bacterial infection could in turn benefit the host to combat pathogens

357 actively.

358

359 Plin1 is an important protein factor on the surface of LDs. It has been reported to control
360 the mobilization of lipids on LDs' surface by recruiting kinds of enzymes (85, 86) and
361 sufficient to alter the morphology of LDs (27). In this study, we found that the
362 expression of *plin1* rather than *plin2* preferred to be regulated by innate immune
363 signaling. This provokes us to conceive that Plin1 may serve as a bridge to link
364 immunity and lipid metabolism through modification of LDs. In response to transient
365 immune activation, adaptative enlarged LDs benefit the host against pathogens and
366 inflammation-induced stress. The alternation of the levels of mammalian PlINs protein
367 on LDs' surface was once mentioned after LPS stimulation (13). Our study provide a
368 possibility that perilipins might response to immune signals and play an active role in
369 infectious pathogenesis through transforming LDs. It is worthy in the future to trace
370 and dissect the dynamic protein compositions on the surface of LDs along the different
371 stages of inflammation, especially the proteins interact with Plin1. In summary, we
372 found that the Plin1-mediated LDs' morphological alteration is not only an adaptive
373 consequence after bacterial infection, but also actively contributes to pathogenic
374 regulation. Therefore, reconfiguration of LDs may provide a potential therapeutic target
375 for resolution of inflammation.

376

377 **Materials and Methods**

378 **Drosophila stocks and bacterial strain.**
379 All flies were propagated at 25˚C on standard cornmeal food (1 L food contains 77.7 g

380 cornmeal, 32.19 g yeast, 10.6 g agar, 0.726 g CaCl2, 31.62 g sucrose,63.2 g glucose, 2
381 g potassium sorbate and 15 ml 5% Tegosept),30%-55% humidity with a 12h/12h
382 light/dark cycle. Fly resources that were used in this study as follows: w^{1118} were used
383 as wild-type controls if no additional indication. *plin1*^{38}, *UAS-plin1* mcherry, *UAS-plin1*
384 *RNAi* and *ppl-GAL4* were kindly gifted from Dr. Xun Huang (Institute of Genetics and
385 Developmental Biology, CAS). *UAS-gstD-GFP* was kindly gifted from Dr. ZhiWei Liu
386 (Shanghai Ocean University). *w*^{1118}, *w[1118];P{w[+mW.hs]=Switch1}106*, *PGRP-L*$^{\Delta}$
387 ^{5}*,Relish*^{E20} were obtained from Bloomington stock center. All flies used in this study
388 were male. Two bacterial strain, *E. coli* (*DH5a*) and *S. typhimurium (SR-11)* (a gift from
389 Dr. ZhiHua Liu, Institute of Biophysics, CAS) were used in this study.
390
391 **Cloning and double-strand RNAs**
392 To construct the *mrt* and *pzg* reporter vector (*mrt*-luc and *pzg*-luc), the *mrt* and *pzg*
393 promoter sequence (about -1500 bp or -1000 bp to 0 bp) was PCR amplified from
394 Drosophila genomic DNA and introduced into *pGL3* vector (Progema) at HindIII
395 restriction site by using recombination technology (Hieff Clone® Plus One Step
396 Cloning Kit, YEASEN). All the plasmid constructs were verified by nucleotide
397 sequencing. *pAC5.1*-renilla plasmid as a normalized reporter. Double-stranded RNAs
398 (dsRNAs) against relish or GFP used in the luciferase reporter assay were synthesized
399 using MEGAscript T7 kit (Invitrogen). Primers used for PCR amplification are listed
400 in Supplementary Table 1.
401
402 **Infection and survival rate counting**
403 Bacterial strains used in this study are *E. coli* (*DH5a*) and *Salmonella typhimurium* (*S.*
404 *typhimurium*). Two days before infection, both bacteria from glycerol stocks were
405 streaked onto Luria Broth (LB) agar plates and grown overnight at 37℃. The plate
406 could be stored at 4 °C for up to 1 week. A single colony was inoculated to 6 ml fresh
407 LB medium and grown at 37°C with shaking (200 rpm). Grow the bacteria to an OD600
408 of 0.7 to 0.8 (about 3.5 hours). The bacterial culture was pelleted with sterile phosphate-
409 buffered saline (PBS) to the desired concentration. We injected 50.6 nl of bacterial
410 suspension into dorsal prothorax of each fly with Nanoject II injector (Drummond). All
411 flies used were 1 week old after eclosion. The final optical density (O.D. / ml) at 600
412 nm for injection were *E. coli* (O.D. 10) and *S. typhimurium* (O.D. 6 or O.D. 3). For
413 *E.coli* infection, each fly obtained about 1x10^6 CFUs. For *S. typhimurium* infection,
414 each fly obtained the lower dose (about 2x10^5 CFUs) or the higher dose (about 1x10^6
415 CFUs) according to the experiment design. Infected flies about 23 per vial were
416 maintained at 25°C. Death was recorded at the indicated time point, and alive flies were
417 transferred to fresh food every day for the survival analysis and CFUs assay.
418
419 **Bacterial loads assay**
420 To monitor bacterial loads of the flies during infection, the number of colony forming
421 units (CFUs) grown on LB agar plate was determined as follow: 5 living flies were
422 randomly collected in a 1.5 ml EP tube, rinsed with 70% ethanol two times by vertex
423 for 10s to sterile the surface adherent bacteria, then rinsed with sterile deionized water

two times by vertex for 10 s, and then homogenized in 200 μl of sterile PBS with three fly body volumes of ceramic beads (diameter: 0.5 mm) in the Minilys apparatus (Bertin TECHNOLOGIES) at highest speed for 30 s. The suspensions obtained were then serially diluted in PBS and plated on LB agar. Specially noted for *S. typhimurium* plating, PBS was substituted with PBS + 1% Triton X-100. For the bacterial load at zero time point, flies were allowed to rest for 10 min after bacterial injection before plating as described above. The agar plate was maintained at 37℃ for 18 hours before CFUs counting. CFUs were $\log_{10}$ transformed.

Cell culture, transfection and luciferase assay

S2* cells (a gift from Dahua Chen, Institute of Zoology, CAS) were maintained in Drosophila Schneider's Medium (Invitrogen) supplemented with 10% heat-inactivated fetal bovine serum (Gibco), 100 units/ml of penicillin, and 100 mg/ml of streptomycin at 28°C. Transient transfection of various plasmids, dsRNA was performed with lipofectamine 3000 (Invitrogen), according to the manufacturer's manual. Luciferase reporter assays were carried out using a dual-luciferase reporter assay system (Promega). Where indicated, cells were treated with PGN (35 μg/μl, 6 h) purified from Erwinia carotovora carotovora 15 (*Ecc15*) referring to previous study(87).

qRT-PCR

For quantification of mRNA level, about 20 flies carcass/fat body tissue were dissected in sterile PBS buffer on ice at indicated time points post infection, immediately homogenized in 200 μl cold TRIzol with three fly body volumes of ceramic beads (diameter: 0.5 mm), then supplied additional 300 μl TRIzol to reach total 500 μl volume and samples were stored at -80℃.RNA extraction was referred to the manual of commercial kit (Magen, Hipure Total RAN Plus Micro Kit), this kit can effectively remove genomic DNA contamination. cDNA was synthesized by using the kit (abm, 5X All-In-One MasterMix) with total 1μg isolated RNA as template in a 20 μl reaction system. Quantitative real-time PCR (qRT-PCR) was performed using a SYBR green kit (abm, EvaGreen supermaster Mix) on an ABI 7500 or ViiATM 7 thermocycler (Life Technology). Samples from at least four independent biological replicates per genotype were collected and analyzed. House-keeping gene rp49 as the reference gene for data normalization. Primer data for qRT-PCR are provided in Supplementary Table 1.

Lipid droplet staining and counting

For lipid droplet staining, adult male carcass/fat body tissues were dissected and fixed in 4% fresh prepared paraformaldehyde (PH=7.5) in PBS for 10 min on ice. Tissues were then rinsed twice with PBS (3 min each time), then incubated in PBS containing 1μg/ml of BODIPY 493/503(Invitrogen) dye or 0.5 μg/ml Nile Red (Sigma) for 30 min on ice, DAPI (1μg/μl, final concentration) was added to stain nuclei at last 5 mins of staining process. After staining, tissues were rinsed three times with PBS (3 mins each time), then mounted in mounting medium (Vector, H-1000) for microscopy analysis. To quantify the average lipid droplet size, the average diameter of the three largest lipid droplets per cell was measured generally, with the exception of *plin1* deficiency

468 associated flies, we measured their biggest lipid droplets in one cell (27). 30 fat body
469 cells of each genotype fly randomly selected from eight confocal images were used to
470 analysis the lipid droplet size. To count the size distribution of lipid droplets, the
471 average percentage of the indicated size range of lipid droplets per cell from 30 fat body
472 cells were determined by using the "Analyze Particles" tool embedded in ImageJ
473 software (https://imagej.nih.gov/ij/). To quantify the fluorescence intensity of GFP on
474 the surface of lipid droplets, confocal images acquired from eight fat bodies were
475 measured by ImageJ software.
476
477 **Glyceride detection**
478 Glyceride amounts were measured using a TG Quantification Kit (BIOSINO, TG kit).
479 Briefly, for whole body glyceride quantification, groups of 12 one-week old male flies
480 were collected and weighted (about 10 mg) in a 1.5 ml EP tube, then immediately stored
481 at -80°C for subsequent assay. Stored flies were homogenized in 200 μl lysis buffer
482 (10mM KH_2PO4, 1mM EDTA, PH=7.4) with three fly body volumes of ceramic beads,
483 and inactivated in water bath at 75°C for 15 min. The inactivated homogenate was
484 homogenized again for 30 s and kept on ice ready for assay. For each glyceride
485 measurement, 3 μl of homogenate was incubated with 250 μl reaction buffer at 37°C
486 for 10 min. After removal debris by centrifugation (2000 rpm, 2 min), 150 μl of clear
487 supernatant was used to perform a colorimetric assay in 96 well plate (Corning® Costar)
488 for absorbance reading at 505 nm. Glyceride level was normalized with fly weight in
489 each homogenate (unit: nmol/mg.fly). For fat body glyceride quantification, 25 fly's
490 carcass/fat body tissues were dissected and following assay as described above.
491 Glyceride level was normalized with per 25 flies (unit: nmol/25.fly).
492
493 **RU486 treatment**
494 RU486 induction was described as before (88). Briefly, A 10 mg/ml stock solution of
495 RU486 (mifepristone; Sigma) was dissolved in DMSO. Appropriate volumes of RU486
496 stock solution was diluted with water containing 2% ethanol to final concentration of
497 50 μg/ml.100 μl of the diluted RU486 solution was dipped onto the surface of fresh
498 food in vials (Diameter: 2 cm). The vials were then allowed to dry at room temperature
499 for half day or 4°C for overnight. Flies were transferred to RU486-contained food and
500 raised in 25°C and fresh food was changed every two days.
501
502 **NAC Treatment**
503 N-acetyl-L-cysteine (NAC) (Beyotime) fresh solution was prepared by dissolving 0.5
504 g of NAC powder in 10 ml distilled water, the solution could be aliquoted into 1 ml per
505 EP tube and frozen or stored at -80 °C. 100 μl of NAC solution was dipped onto the
506 surface of fresh food in vials (Diameter: 2 cm). The vials were then allowed to dry at
507 room temperature for half day or 4°C for overnight. Flies were transferred to NAC-
508 contained food and raised in 25°C and fresh food was changed every day.
509
510 **ROS detection**
511 We used two methods to detect ROS in fat body, which are *gstD-GFP* reporter flies and

512 dichlorofluorescein diacetate (DCFH-DA) labeling. The oxidative stress reporter
513 construct *gstD-GFP* for evaluating cellular ROS levels has been describe before (58).
514 Briefly, the carcass/fat body of transgenic flies containing a *gstD-GFP* reporter
515 construct were dissected in sterile PBS, fixed in 4% formaldehyde for 10 min on ice,
516 rinsed twice with ice-chilled PBS (3 min each time), then the flaky fat body cells
517 attached to the inner carcass shell were dissected out to mount and confocal image
518 (Vector, H-1000). DCFH-DA (Beyotime, Reactive Oxygen Species Assay Kit) labeling
519 of fresh dissected carcass/fat body tissues was performed according to the
520 manufacturer's manual, which based on the ROS-dependent oxidation of DCFH-DA to
521 fluorescent molecule 2'-7'dichlorofluorescein (DCF). In brief, the tissues were
522 incubated with PBS containing 20 μM DCFH-DA for 30 min at 30℃, washed with
523 sterile PBS for three times (3 min each) to remove free DCFH-DA that do not uptake
524 by the cell, then the flaky fat body cells attached to the inner carcass shell immediately
525 were dissected out to mount and confocal image (Vector, H-1000). It should be noted
526 that the slices were confocal imaged using the exact same settings for control and
527 experimental groups. The fluorescence intensity is proportional to the ROS levels,
528 fluorescence intensity of GFP or DCF was quantified by using ImageJ software.
529
530 **Microscopy and software**
531 LSM700 (Leica) and Olympus FV-1200 confocal laser scanning microscopy were used
532 for imaging. Captured images were analyzed by implemented soft respectively. ImageJ
533 (https://imagej.nih.gov/ij/) was used for analysis of fluorescence intensity and lipid
534 droplets size.
535
536 **Statistical analyses**
537 All replicates are showed as the mean ± SD or mean with range. Statistical significance
538 was determined using a paired Student's t-test for two measurements, one-way ANOVA
539 (Tukey's HSD) with a multiple t-tests and Multiple t-tests for pairwise comparisons.
540 Kaplan–Meier test for survival curves comparison. All data processing was used with
541 GraphPad Prism 7.0.
542
543 *Sample size choice.* The sample size was determined according to the number of data
544 points. Batches of experiment were carried out to ensure repeatability and the use of
545 enough animals for each data point.
546
547 *Randomization.* Measures were taken to ensure randomization. Each experimental
548 batch contained more animals than the number of data points, to ensure randomization
549 and the accidental exclusion of animals. In vitro analyses were usually performed on a
550 specimen from animals at each data point to ensure a minimum of three biological
551 replicates.
552
553 *Blinding.* Data collection and data analysis were routinely performed by different
554 people to blind potential bias. All measurement data are expressed as mean ± s.d. to
555 maximally show derivations, unless otherwise specified.

556

557 **Acknowledgements**

558 We thank Drs. Xun Huang (Institute of Genetics and Developmental Biology, CAS) for
559 providing stocks of *plin1*^{38}, *UAS-plin1*-mcherry, *UAS-plin1-RNAi* flies and valuable
560 comments; Zhiwei Liu (Shanghai Ocean University) for providing stock of *UAS-gstD-*
561 *GFP*; Zhihua Liu (Institute of Biophysics, CAS) for providing *S. typhimurium (SR-11)*
562 strain; Ms. Song-qing Liu (Institute of Biophysics, CAS) for fly food preparation and
563 stock maintenance. We thank Drs. Hui Xiao, Parag Kundu and Philippe Sansonetti (IPS,
564 CAS) and Chengshu Wang (SIPPE,CAS) for comments and manuscript polishment.
565 This work was supported by grants from the Strategic Priority Research Program of the
566 Chinese Academy of Sciences to H.T (XDB29030301), the National Natural Science
567 Foundation of China to L.P (31870887) and J.Y (31670909) and Shanghai Municipal
568 Science and Technology Major Project to L.P (2019SHZDZX02). L.P is a fellow of
569 CAS Youth Innovation Promotion Association (2012083).

570

571 **Author's contributions**

572 Conceptualization, L.W., J.L. and L.P.; Methodology and Validation, L.W., J.L., L.S.,
573 K.Y. and L.P.; Formal Analysis, L.W. J.L., J.Y., and L.P.; Investigation, L.W., J.L. and
574 L.P.; Resources, L.P.; Writing-Original Draft, L.W. and L.P.; Writing -Review & Editing,
575 L.P.; Supervision, H.T. and L.P.; Funding Acquisition, J.Y., H.T. and L.P.

576

577 **DECLARATION OF INTERESTS**

578 The authors declare no competing interests.

579

580 **References**

581 1. Hotamisligil G. 2017. Foundations of Immunometabolism and Implications for Metabolic
582 Health and Disease. Immunity 3:406-420.
583 2. O'Neill LA, Kishton RJ, Rathmell J. 2016. A guide to immunometabolism for immunologists. Nat
584 Rev Immunol 16:553-65.
585 3. Arita M. 2012. Mediator lipidomics in acute inflammation and resolution. J Biochem 152:313-
586 9.
587 4. Serhan CN, Chiang N, Dalli J, Levy BD. 2014. Lipid mediators in the resolution of inflammation.
588 Cold Spring Harb Perspect Biol 7:a016311.
589 5. Walpole GFW GS, Westman J. 2018. The Role of Lipids in Host–PathogenInteractions. IUBMB
590 Life 5:384-392.
591 6. Murphy D. 2001. The biogenesis and functions of lipid bodies in animals, plants and
592 microorganisms. Prog Lipid Res 5:325-438.
593 7. Tauchi-Sato K, Ozeki S, Houjou T, Taguchi R, Fujimoto T. 2002. The surface of lipid droplets is a
594 phospholipid monolayer with a unique Fatty Acid composition. J Biol Chem 277:44507-12.
595 8. Walther TC, Farese RV, Jr. 2012. Lipid droplets and cellular lipid metabolism. Annu Rev Biochem
596 81:687-714.
597 9. Olzmann JA, Carvalho P. 2019. Dynamics and functions of lipid droplets. Nat Rev Mol Cell Biol
598 20:137-155.
599 10. den Brok MH, Raaijmakers TK, Collado-Camps E, Adema GJ. 2018. Lipid Droplets as Immune
600 Modulators in Myeloid Cells. Trends Immunol 39:380-392.
601 11. Hinson ER, Cresswell P. 2009. The antiviral protein, viperin, localizes to lipid droplets via its N-
602 terminal amphipathic alpha-helix. Proc Natl Acad Sci U S A 106:20452-7.
603 12. Anand P, Cermelli S, Li Z, Kassan A, Bosch M, Sigua R, Huang L, Ouellette AJ, Pol A, Welte MA,
604 Gross SP. 2012. A novel role for lipid droplets in the organismal antibacterial response. Elife
605 1:e00003.
606 13. Bosch M, Sanchez-Alvarez M, Fajardo A, Kapetanovic R, Steiner B, Dutra F, Moreira L, Lopez JA,
607 Campo R, Mari M, Morales-Paytuvi F, Tort O, Gubern A, Templin RM, Curson JEB, Martel N,
608 Catala C, Lozano F, Tebar F, Enrich C, Vazquez J, Del Pozo MA, Sweet MJ, Bozza PT, Gross SP,
609 Parton RG, Pol A. 2020. Mammalian lipid droplets are innate immune hubs integrating cell
610 metabolism and host defense. Science 370.
611 14. Pereira-Dutra FS, Teixeira L, de Souza Costa MF, Bozza PT. 2019. Fat, fight, and beyond: The
612 multiple roles of lipid droplets in infections and inflammation. J Leukoc Biol
613 doi:10.1002/JLB.4MR0119-035R.
614 15. Henne WM, Reese ML, Goodman JM. 2018. The assembly of lipid droplets and their roles in
615 challenged cells. EMBO J 37.
616 16. Menon D, Singh K, Pinto SM, Nandy A, Jaisinghani N, Kutum R, Dash D, Prasad TSK, Gandotra
617 S. 2019. Quantitative Lipid Droplet Proteomics Reveals Mycobacterium tuberculosis Induced
618 Alterations in Macrophage Response to Infection. ACS Infect Dis 5:559-569.
619 17. Harsh S, Heryanto C, Eleftherianos I. 2019. Intestinal lipid droplets as novel mediators of host-

620 pathogen interaction in Drosophila. Biol Open 8.
621 18. Ertunc ME, Hotamisligil GS. 2016. Lipid signaling and lipotoxicity in metaflammation:
622 indications for metabolic disease pathogenesis and treatment. J Lipid Res 57:2099-2114.
623 19. Listenberger LL, Han X, Lewis SE, Cases S, Farese RV, Jr., Ory DS, Schaffer JE. 2003. Triglyceride
624 accumulation protects against fatty acid-induced lipotoxicity. Proc Natl Acad Sci U S A
625 100:3077-82.
626 20. Feldstein AE, Werneburg NW, Canbay A, Guicciardi ME, Bronk SF, Rydzewski R, Burgart LJ, Gores
627 GJ. 2004. Free fatty acids promote hepatic lipotoxicity by stimulating TNF-alpha expression via
628 a lysosomal pathway. Hepatology 40:185-94.
629 21. Summers SA. 2006. Ceramides in insulin resistance and lipotoxicity. Prog Lipid Res 45:42-72.
630 22. Guo Y, Walther TC, Rao M, Stuurman N, Goshima G, Terayama K, Wong JS, Vale RD, Walter P,
631 RV. F. 2008. Functional genomic screen reveals genes involved in lipid-droplet formation and
632 utilization. Nature 7195:657-61.
633 23. Beller M, Riedel D, Jänsch L, Dieterich G, Wehland J, Jäckle H, RP. K. 2006. Characterization of
634 the Drosophila lipid droplet subproteome. Mol Cell Proteomics 6:1082-94.
635 24. Itabe H, Yamaguchi T, Nimura S, Sasabe N. 2017. Perilipins: a diversity of intracellular lipid
636 droplet proteins. Lipids Health Dis 16:83.
637 25. Kimmel AR, Sztalryd C. 2016. The Perilipins: Major Cytosolic Lipid Droplet-Associated Proteins
638 and Their Roles in Cellular Lipid Storage, Mobilization, and Systemic Homeostasis. Annu Rev
639 Nutr 36:471-509.
640 26. Sztalryd C, Brasaemle DL. 2017. The perilipin family of lipid droplet proteins: Gatekeepers of
641 intracellular lipolysis. Biochim Biophys Acta Mol Cell Biol Lipids 1862:1221-1232.
642 27. Bi J, Xiang Y, Chen H, Liu Z, Gronke S, Kuhnlein RP, Huang X. 2012. Opposite and redundant roles
643 of the two Drosophila perilipins in lipid mobilization. J Cell Sci 125:3568-77.
644 28. Beller M, Bulankina AV, Hsiao HH, Urlaub H, Jackle H, Kuhnlein RP. 2010. PERILIPIN-dependent
645 control of lipid droplet structure and fat storage in Drosophila. Cell Metab 12:521-32.
646 29. Gandotra S LDC, Bottomley W, Cervera P, Giral P, Reznik Y, Charpentier G, Auclair M, Delépine
647 M, Barroso I, Semple RK, Lathrop M, Lascols O, Capeau J, O'Rahilly S, Magré J, Savage DB,
648 Vigouroux C. 2011. Perilipin Deficiency and Autosomal Dominant Partial Lipodystrophy. N
649 Engl J Med 8:740.
650 30. Tansey JT, Sztalryd C, Gruia-Gray J, Roush DL, Zee JV, Gavrilova O, Reitman ML, Deng CX, Li C,
651 Kimmel AR, Londos C. 2001. Perilipin ablation results in a lean mouse with aberrant adipocyte
652 lipolysis, enhanced leptin production, and resistance to diet-induced obesity. Proc Natl Acad
653 Sci U S A 98:6494-9.
654 31. Schweiger M, Romauch M, Schreiber R, Grabner GF, Hutter S, Kotzbeck P, Benedikt P, Eichmann
655 TO, Yamada S, Knittelfelder O, Diwoky C, Doler C, Mayer N, De Cecco W, Breinbauer R,
656 Zimmermann R, Zechner R. 2017. Pharmacological inhibition of adipose triglyceride lipase
657 corrects high-fat diet-induced insulin resistance and hepatosteatosis in mice. Nat Commun
658 8:14859.
659 32. Cani PD, Amar J, Iglesias MA, Poggi M, Knauf C, Bastelica D, Neyrinck AM, Fava F, Tuohy KM,
660 Chabo C, Waget A, Delmee E, Cousin B, Sulpice T, Chamontin B, Ferrieres J, Tanti JF, Gibson GR,
661 Casteilla L, Delzenne NM, Alessi MC, Burcelin R. 2007. Metabolic endotoxemia initiates obesity
662 and insulin resistance. Diabetes 56:1761-72.
663 33. Sohn JH, Lee YK, Han JS, Jeon YG, Kim JI, Choe SS, Kim SJ, Yoo HJ, Kim JB. 2018. Perilipin 1 (Plin1)

664 deficiency promotes inflammatory responses in lean adipose tissue through lipid dysregulation.
665 J Biol Chem doi:10.1074/jbc.RA118.003541.
666 34. Heier C, Kuhnlein RP. 2018. Triacylglycerol Metabolism in Drosophila melanogaster. Genetics
667 210:1163-1184.
668 35. Lemaitre B, Hoffmann J. 2007. The host defense of Drosophila melanogaster. Annu Rev
669 Immunol 25:697-743.
670 36. Myllymaki H, Valanne S, Ramet M. 2014. The Drosophila imd signaling pathway. J Immunol
671 192:3455-62.
672 37. Arrese EL, Soulages JL. 2010. Insect fat body: energy, metabolism, and regulation. Annu Rev
673 Entomol 55:207-25.
674 38. Kleino A, Silverman N. 2014. The Drosophila IMD pathway in the activation of the humoral
675 immune response. Dev Comp Immunol 42:25-35.
676 39. Bickel PE, Tansey JT, Welte MA. 2009. PAT proteins, an ancient family of lipid droplet proteins
677 that regulate cellular lipid stores. Biochim Biophys Acta 1791:419-40.
678 40. Fauny JD, Silber J, Zider A. 2005. Drosophila Lipid Storage Droplet 2 gene (Lsd-2) is expressed
679 and controls lipid storage in wing imaginal discs. Dev Dyn 232:725-32.
680 41. Grönke S, Beller M, Fellert S, Ramakrishnan H, Jäckle H, Kühnlein RP. 2003. Control of Fat
681 Storage by a Drosophila PAT Domain Protein. Current Biology 13:603-606.
682 42. Teixeira Ls, Rabouille C, Rørth P, Ephrussi A, Vanzo NF. 2003. Drosophila Perilipin/ADRP
683 homologue Lsd2 regulates lipid metabolism. Mechanisms of Development 120:1071-1081.
684 43. Molaei M, Vandehoef C, Karpac J. 2019. NF-kappaB Shapes Metabolic Adaptation by
685 Attenuating Foxo-Mediated Lipolysis in Drosophila. Dev Cell 49:802-810 e6.
686 44. Kamareddine L, Robins WP, Berkey CD, Mekalanos JJ, Watnick PI. 2018. The Drosophila Immune
687 Deficiency Pathway Modulates Enteroendocrine Function and Host Metabolism. Cell Metab
688 28:449-462 e5.
689 45. Leulier F, Parquet C, Pili-Floury S, Ryu JH, Caroff M, Lee WJ, Mengin-Lecreulx D, Lemaitre B.
690 2003. The Drosophila immune system detects bacteria through specific peptidoglycan
691 recognition. Nat Immunol 4:478-84.
692 46. Neyen C, Runchel C, Schüpfer F, Meier P, Lemaitre B. 2016. The regulatory isoform rPGRP-LC
693 induces immune resolution via endosomal degradation of receptors. Nat Immunol 17:1150-8.
694 47. Vodovar N, Vinals M, Liehl P, Basset A, Degrouard J, Spellman P, Boccard F, Lemaitre B. 2005.
695 Drosophila host defense after oral infection by an entomopathogenic Pseudomonas species.
696 Proc Natl Acad Sci U S A 102:11414-9.
697 48. Kühnlein. 2012. Thematic review series: Lipid droplet synthesis and metabolism: from yeast to
698 man. Lipid droplet-based storage fat metabolism in Drosophila. J Lipid Res 53(8):1430-6.
699 49. Yao Y, Li X, Wang W, Liu Z, Chen J, Ding M, Huang X. 2018. MRT, Functioning with NURF Complex,
700 Regulates Lipid Droplet Size. Cell Rep 24:2972-2984.
701 50. Kaneko T GW, Mellroth P, Steiner H, Fukase K, Kusumoto S, Harley W, Fox A, Golenbock D,
702 Silverman N. 2004. Monomeric and polymeric gram-negative peptidoglycan but not purified
703 LPS stimulate the Drosophila IMD pathway. Immunity 20:637-49.
704 51. He X, Yu J, Wang M, Cheng Y, Han Y, Yang S, Shi G, Sun L, Fang Y, Gong ST, Wang Z, Fu YX, Pan L,
705 Tang H. 2017. Bap180/Baf180 is required to maintain homeostasis of intestinal innate immune
706 response in Drosophila and mice. Nat Microbiol 2:17056.
707 52. Brandt SM, Dionne MS, Khush RS, Pham LN, Vigdal TJ, Schneider DS. 2004. Secreted Bacterial

708 Effectors and Host-Produced Eiger/TNF Drive Death in aSalmonella-Infected Fruit Fly. PLoS Biol
709 2:e418.
710 53. Morgan MJ, Liu ZG. 2011. Crosstalk of reactive oxygen species and NF-kappaB signaling. Cell
711 Res 21:103-15.
712 54. Herms A, Bosch M, Ariotti N, Reddy BJ, Fajardo A, Fernandez-Vidal A, Alvarez-Guaita A,
713 Fernandez-Rojo MA, Rentero C, Tebar F, Enrich C, Geli MI, Parton RG, Gross SP, Pol A. 2013.
714 Cell-to-cell heterogeneity in lipid droplets suggests a mechanism to reduce lipotoxicity. Curr
715 Biol 23:1489-96.
716 55. C M Griswold, A L Matthews, K E Bewley, Mahaffey JW. 1993. Molecular Characterization and
717 Rescue of Acatalasemic Mutants of Drosophila Melanogaster. Genetics 134(3):781-8.
718 56. J P Phillips , S D Campbell, D Michaud, M Charbonneau, Hilliker AJ. 1989. Null Mutation of
719 Copper-Zinc Superoxide Dismutase in Drosophila Confers Hypersensitivity to Paraquat and
720 Reduced Longevity. Proc Natl Acad Sci 86(8):2761-5.
721 57. Blaser H, Dostert C, Mak TW, Brenner D. 2016. TNF and ROS Crosstalk in Inflammation. Trends
722 Cell Biol 26:249-261.
723 58. Sykiotis GP, Bohmann D. 2008. Keap1/Nrf2 signaling regulates oxidative stress tolerance and
724 lifespan in Drosophila. Dev Cell 14:76-85.
725 59. Ha EM, Oh CT, Bae YS, Lee WJ. 2005. A direct role for dual oxidase in Drosophila gut immunity.
726 Science 310:847-50.
727 60. Ha EM, Oh CT, Ryu JH, Bae YS, Kang SW, Jang IH, Brey PT, Lee WJ. 2005. An antioxidant system
728 required for host protection against gut infection in Drosophila. Dev Cell 8:125-32.
729 61. Buck MD, Sowell RT, Kaech SM, Pearce EL. 2017. Metabolic Instruction of Immunity. Cell
730 169:570-586.
731 62. Peyron P, Vaubourgeix J, Poquet Y, Levillain F, Botanch C, Bardou F, Daffe M, Emile JF, Marchou
732 B, Cardona PJ, de Chastellier C, Altare F. 2008. Foamy macrophages from tuberculous patients'
733 granulomas constitute a nutrient-rich reservoir for M. tuberculosis persistence. PLoS Pathog
734 4:e1000204.
735 63. D'Avila H, Melo RCN, Parreira GG, Werneck-Barroso E, Castro-Faria-Neto HC, Bozza PT. 2006.
736 Mycobacterium bovis Bacillus Calmette-Guerin Induces TLR2-Mediated Formation of Lipid
737 Bodies: Intracellular Domains for Eicosanoid Synthesis In Vivo. The Journal of Immunology
738 176:3087-3097.
739 64. Samsa MM, Mondotte JA, Iglesias NG, Assuncao-Miranda I, Barbosa-Lima G, Da Poian AT, Bozza
740 PT, Gamarnik AV. 2009. Dengue virus capsid protein usurps lipid droplets for viral particle
741 formation. PLoS Pathog 5:e1000632.
742 65. Barba G HF, Harada T, Kohara M, Goulinet S, Matsuura Y, Eder G, Schaff Z, Chapman MJ,
743 Miyamura T, Bréchot C. 1997. Hepatitis C virus core protein shows a cytoplasmic localization
744 and associates to cellular lipid storage droplets. Proc Natl Acad Sci U S A 94:1200-5.
745 66. Hope RG, Murphy DJ, McLauchlan J. 2002. The domains required to direct core proteins of
746 hepatitis C virus and GB virus-B to lipid droplets share common features with plant oleosin
747 proteins. J Biol Chem 277:4261-70.
748 67. Sorgi CA, Secatto A, Fontanari C, Turato WM, Belanger C, de Medeiros AI, Kashima S, Marleau
749 S, Covas DT, Bozza PT, Faccioli LH. 2009. Histoplasma capsulatum cell wall {beta}-glucan induces
750 lipid body formation through CD18, TLR2, and dectin-1 receptors: correlation with leukotriene
751 B4 generation and role in HIV-1 infection. J Immunol 182:4025-35.

752 68. Vallochi AL, Teixeira L, Oliveira KDS, Maya-Monteiro CM, Bozza PT. 2018. Lipid Droplet, a Key
753 Player in Host-Parasite Interactions. Front Immunol 9:1022.
754 69. Pacheco P, Bozza FA GR, Bozza M WP, Castro-Faria-Neto HC, PT. B. 2002. Lipopolysaccharide-
755 induced leukocyte lipid body formation in vivo innate immunity elicited intracellular Loci
756 involved in eicosanoid metabolism.pdf>. J Immunol 1:6498-506.
757 70. Bandeira-Melo C, Phoofolo M, Weller PF. 2001. Extranuclear lipid bodies, elicited by CCR3-
758 mediated signaling pathways, are the sites of chemokine-enhanced leukotriene C4 production
759 in eosinophils and basophils. J Biol Chem 276:22779-87.
760 71. Clark RI, Tan SW, Pean CB, Roostalu U, Vivancos V, Bronda K, Pilatova M, Fu J, Walker DW,
761 Berdeaux R, Geissmann F, Dionne MS. 2013. MEF2 is an in vivo immune-metabolic switch. Cell
762 155:435-47.
763 72. Dionne MS, Pham LN, Shirasu-Hiza M, Schneider DS. 2006. Akt and FOXO dysregulation
764 contribute to infection-induced wasting in Drosophila. Curr Biol 16:1977-85.
765 73. Song Y, Li X, Li Y, Li N, Shi X, Ding H, Zhang Y, Li X, Liu G, Wang Z. 2014. Non-esterified fatty acids
766 activate the ROS-p38-p53/Nrf2 signaling pathway to induce bovine hepatocyte apoptosis in
767 vitro. Apoptosis 19:984-97.
768 74. Koppers AJ, Garg ML, Aitken RJ. 2010. Stimulation of mitochondrial reactive oxygen species
769 production by unesterified, unsaturated fatty acids in defective human spermatozoa. Free
770 Radic Biol Med 48:112-9.
771 75. Aitken RJ, Wingate JK, De Iuliis GN, Koppers AJ, McLaughlin EA. 2006. Cis-unsaturated fatty
772 acids stimulate reactive oxygen species generation and lipid peroxidation in human
773 spermatozoa. J Clin Endocrinol Metab 91:4154-63.
774 76. Krawczyk SA, Haller JF, Ferrante T, Zoeller RA, BE C. 2012. Reactive Oxygen Species Facilitate
775 Translocation of Hormone Sensitive Lipase to the Lipid Droplet During Lipolysis in Human
776 Differentiated Adipocytes. PLoS ONE 7:e34904.
777 77. Li X, Rommelaere S, Kondo S, Lemaitre B. 2020. Renal Purge of Hemolymphatic Lipids Prevents
778 the Accumulation of ROS-Induced Inflammatory Oxidized Lipids and Protects Drosophila from
779 Tissue Damage. Immunity 52:374-387 e6.
780 78. Bailey AP, Koster G, Guillermier C, Hirst EM, MacRae JI, Lechene CP, Postle AD, Gould AP. 2015.
781 Antioxidant Role for Lipid Droplets in a Stem Cell Niche of Drosophila. Cell 163:340-53.
782 79. Bensaad K, Favaro E, Lewis CA, Peck B, Lord S, Collins JM, Pinnick KE, Wigfield S, Buffa FM, Li JL,
783 Zhang Q, Wakelam MJO, Karpe F, Schulze A, Harris AL. 2014. Fatty acid uptake and lipid storage
784 induced by HIF-1alpha contribute to cell growth and survival after hypoxia-reoxygenation. Cell
785 Rep 9:349-365.
786 80. LaRock DL, Chaudhary A, Miller SI. 2015. Salmonellae interactions with host processes. Nat Rev
787 Microbiol 13:191-205.
788 81. Narayanan LA, Edelmann MJ. 2014. Ubiquitination as an efficient molecular strategy employed
789 in salmonella infection. Front Immunol 5:558.
790 82. Arena ET, Auweter SD, Antunes LC, Vogl AW, Han J, Guttman JA, Croxen MA, Menendez A, Covey
791 SD, Borchers CH, Finlay BB. 2011. The deubiquitinase activity of the Salmonella pathogenicity
792 island 2 effector, SseL, prevents accumulation of cellular lipid droplets. Infect Immun 79:4392-
793 400.
794 83. Anand P, Cermelli S LZ, Kassan A, Bosch M SR, Huang L, Ouellette AJ, Pol A, Welte MA, SP. G.
795 2012. A novel role for lipid droplets in the organismal antibacterial response. Elife 13:e00003.

84. Knight M, Braverman J, Asfaha K, Gronert K, Stanley S. 2018. Lipid droplet formation in Mycobacterium tuberculosis infected macrophages requires IFN-gamma/HIF-1alpha signaling and supports host defense. PLoS Pathog 14:e1006874.
85. Gandotra S, Lim K, Girousse A, Saudek V, O'Rahilly S, Savage DB. 2011. Human frame shift mutations affecting the carboxyl terminus of perilipin increase lipolysis by failing to sequester the adipose triglyceride lipase (ATGL) coactivator AB-hydrolase-containing 5 (ABHD5). J Biol Chem 286:34998-5006.
86. Sztalryd C, Xu G, Dorward H, Tansey JT, Contreras JA, Kimmel AR, Londos C. 2003. Perilipin A is essential for the translocation of hormone-sensitive lipase during lipolytic activation. J Cell Biol 161:1093-103.
87. Gottar M GV, Michel T, Belvin M, Duyk G, Hoffmann JA, Ferrandon D, Royet J. 2002. The Drosophila immune response against Gram-negative bacteria is mediated by a peptidoglycan recognition protein. Nature 11:640-4.
88. Poirier L SA, Zheng J, Seroude L. 2008. Characterization of the Drosophila gene-switch system in aging studies: a cautionary tale. Aging Cell 2008 Oct; 7(5).

MAIN FIGURES AND LEGENDS

Including seven main figures.

Figure 1

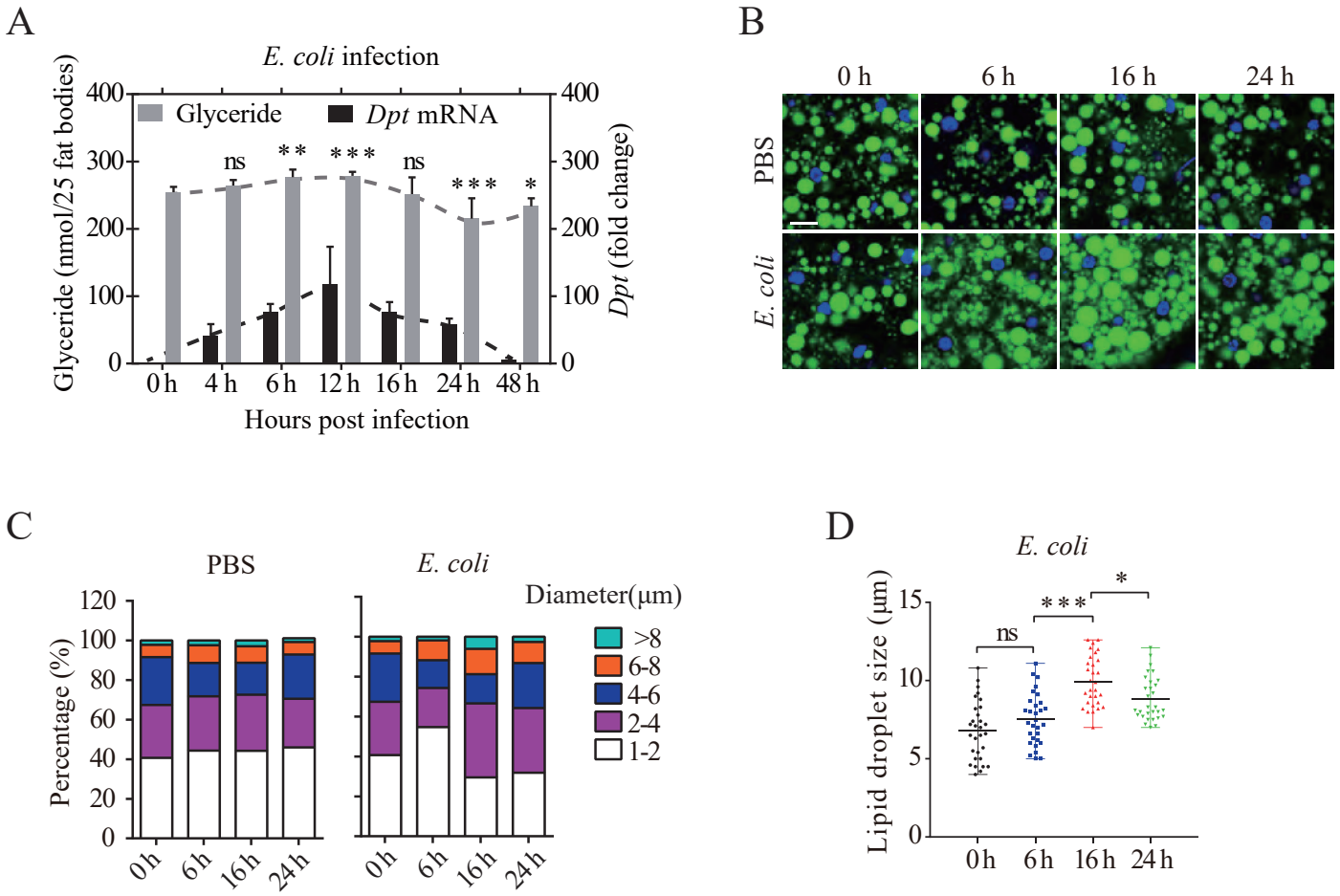
A
E. coli infection
Glyceride
Dpt mRNA
Glyceride (nmol/25 fat bodies)
Dpt (fold change)
ns
**
***
ns
***
*
0 h
4 h
6 h
12 h
16 h
24 h
48 h
Hours post infection
B
0 h
6 h
16 h
24 h
PBS
E. coli
C
PBS
E. coli
Diameter(μm)
>8
6-8
4-6
2-4
1-2
Percentage (%)
0h
6h
16h
24h
D
E. coli
Lipid droplet size (μm)
ns
***
*
0h
6h
16h
24h

Fig. 1. *E. coli* infection switches lipid metabolism and LDs morphology in the fat body. (**A**) Relative *Dptericin*(*Dpt*) mRNA expression and glyceride level in the fat body of wild type flies at indicated time points post *E. coli* infection. The mean values of *Dpt* mRNA expression or glyceride level was connected by dash line. The fold change of mRNA expression was normalized to that of 0 h and four independent repeats (n =20 flies per repeat) were performed at each time point. Total glyceride level of 25 flies' fat body tissues was quantified in six biological replicates at each time point. (**B and C**) BODIPY staining (green) of LDs in the fat body of wild type flies at indicated time points post *E. coli* infection. Nuclei of fat body cells were stained with DAPI (blue). Scale bar: 10 μm. The corresponding statistics of the distribution of LDs' size was shown in (**C**) for *E. coli* infection (n =30 cells for each time point). Eight fat bodies were examined for each time point.(**D**) The statistics of LDs' size (n =30 cells) in the fat body of wild type flies at indicated time point post *E. coli* infection. Each scattering dot represents the data from one fat body cell. Error bars represent the mean ± s.d. (**A-**) and mean with range (**D**). Data were analyzed by One-way ANOVA with Tukey's multiple-comparison test (**A, D**). $*p < 0.05$; $**p < 0.01$; $***p < 0.001$; ns, not significant. **See also in Supplementary Figure 1.**

Figure 2

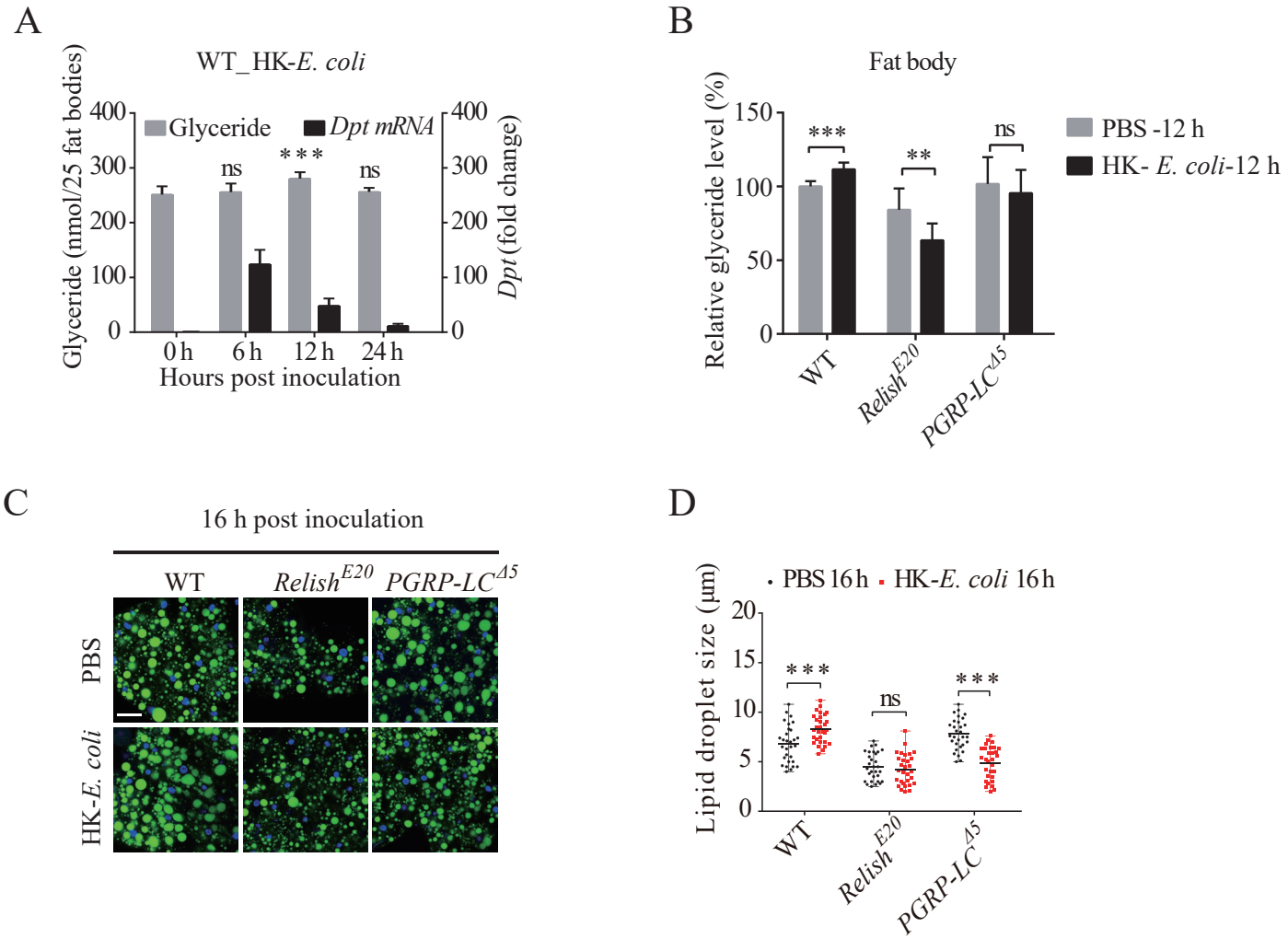
A
WT_HK-E. coli
Glyceride (nmol/25 fat bodies)
Glyceride
Dpt mRNA
Dpt (fold change)
ns
***
ns
0 h
6 h
12 h
24 h
Hours post inoculation
B
Fat body
Relative glyceride level (%)
***
**
ns
PBS -12 h
HK- E. coli-12 h
WT
Relish^E20
PGRP-LC^Δ5
C
16 h post inoculation
WT
Relish^E20
PGRP-LC^Δ5
PBS
HK-E. coli
D
PBS 16 h
HK-E. coli 16 h
Lipid droplet size (μm)
***
ns
***
WT
Relish^E20
PGRP-LC^Δ5

Fig. 2. IMD signaling pathway is required for the alteration of lipid metabolism and LDs morphology upon infection. (**A**) Relative *Dptericin* (*Dpt*) mRNA expression (black) and Fat levels (Grey) in the fat body of wild type flies at indicated time points post heat-killed *E. coli* (HK-*E. coli*) infection. The fold change of mRNA expression was normalized to that of 0 h and four independent repeats (n =20 flies per repeat) were performed at each time point. Total fat levels of 25 flies' fat body tissues was quantified in six biological replicates at each time point. (**B**) Relative glyceride level in the fat body of wild type and IMD pathway mutants (*Relish* and *PGRP-LC*). Each value of glyceride level was normalized to that of 0h of wild type. Each data contains four independent repeats (25 flies' fat body tissues per repeat). (**C** and **D**) BODIPY staining (green) of LDs (**C**) and the corresponding statistics of LDs' size (n =30 cells) (**D**) in the fat body of IMD pathway mutant flies and corresponding genetic control flies. Eight fat bodies were examined for each sample. Error bars represent mean ± s.d. (**A-B**) or mean with range (**D**). Data were analyzed by One-way ANOVA with Tukey's multiple-comparison test (A-B) and Multiple t-tests (D). Scale bar: 20 μm. *$p < 0.05$; ** $p < 0.01$; *** $p < 0.001$; ns, no significance.

Figure 3

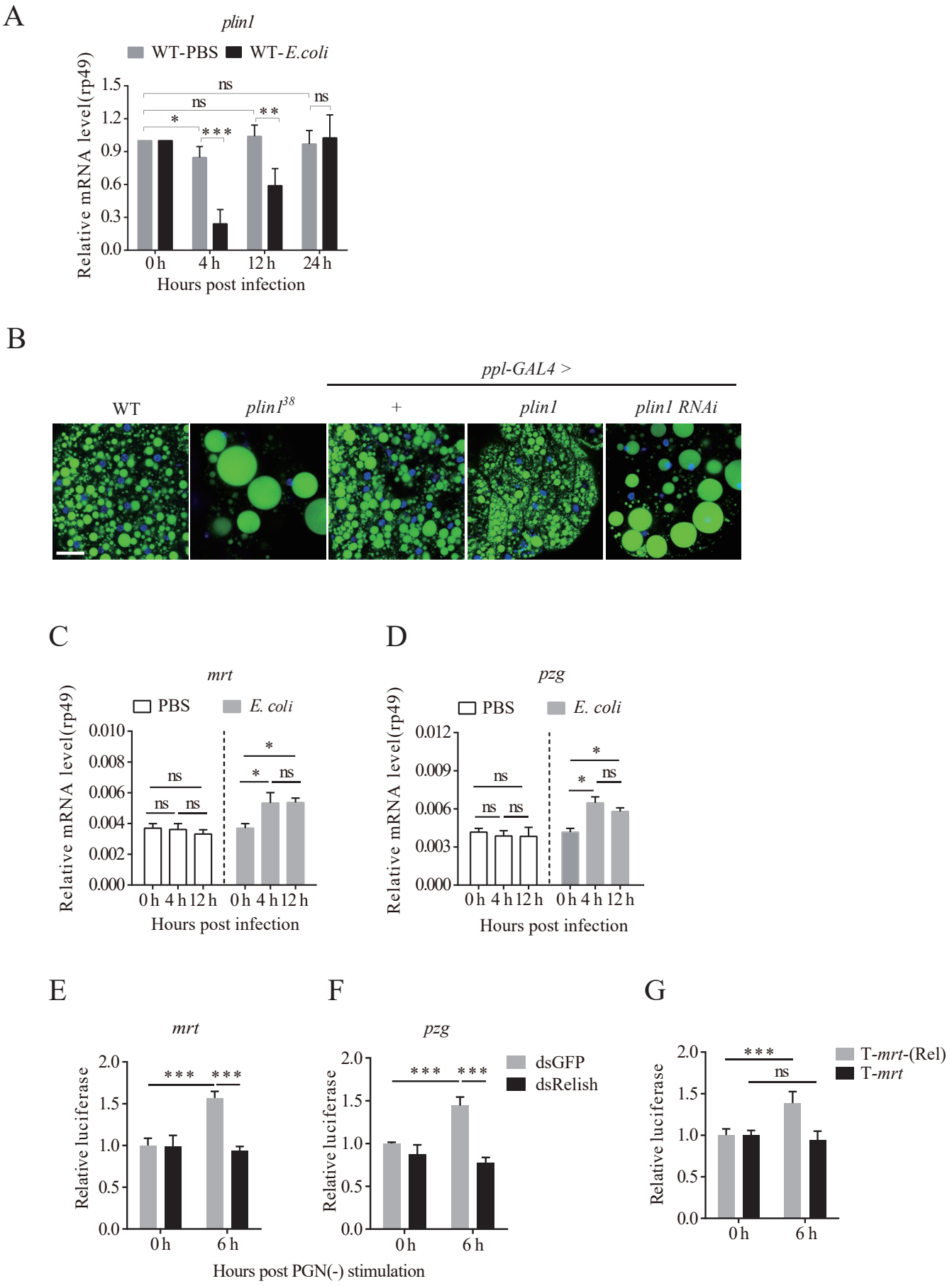
A
plin1
WT-PBS
WT-E.coli
Relative mRNA level(rp49)
1.5
1.2
0.9
0.6
0.3
0.0
ns
ns
ns
*
***
**
0 h
4 h
12 h
24 h
Hours post infection
B
ppl-GAL4 >
WT
plin1^38
+
plin1
plin1 RNAi
C
mrt
PBS
E. coli
Relative mRNA level(rp49)
0.010
0.008
0.006
0.004
0.002
0.000
ns
ns
ns
*
*
ns
0 h 4 h 12 h 0 h 4 h 12 h
Hours post infection
D
pzg
PBS
E. coli
Relative mRNA level(rp49)
0.012
0.009
0.006
0.003
0.000
ns
ns
ns
*
*
ns
0 h 4 h 12 h 0 h 4 h 12 h
Hours post infection
E
mrt
Relative luciferase
2.0
1.5
1.0
0.5
0.0
***
***
0 h
6 h
F
pzg
dsGFP
dsRelish
Relative luciferase
2.0
1.5
1.0
0.5
0.0
***
***
0 h
6 h
Hours post PGN(-) stimulation
G
T-mrt-(Rel)
T-mrt
Relative luciferase
2.0
1.5
1.0
0.5
0.0
***
ns
0 h
6 h

Fig. 3. *plin1* responds to IMD activation through Mrt/Pzg complex, and regulates LDs' morphology. (**A**) Relative *plin1* mRNA levels in the fat body of wild type flies at the indicated time points post *E. coli* infection. Flies treated with sterile PBS were used as a control. The fold change of mRNA expression was normalized to that of 0 h**.** (**B**) BODIPY staining (green) of LDs in the fat body of indicated flies. Nuclei of fat body cells were stained with DAPI (blue). Eight fat bodies were examined for each genotype. (**C** and **D**) Relative *mrt* (**C**) and *pzg* (**D**) mRNA levels in the fat body of wild type flies post *E. coli* infection. Flies treated with sterile PBS were used as a control. The fold change of mRNA expression was normalized to that of 0 h. Four independent repeats (n=20 flies fat body tissues per repeat) were performed at each time point for each group. (**E** and **F**) Relative luciferase activities of *mrt* (**E**) (Full length promoter of -1.5kb to +1bp including all predicted Relish Binding motifs in Fig. S3) reporter or *pzg* (**F**) (1.5 KB upstream of TSS, all predicted Relish binding sites are covered) reporter in S2* cells after double strand RNA (dsRNA) and PGN (35 μg/ml) treatment. All data were normalized to dsGFP control group at 0 h. (**G**) Relative luciferase activities of T-*mrt* (Rel) and T-*mrt* reporter in S2* cells after PGN (35 μg/ml) treatment. All data were normalized to T-*mrt* (Rel) group at 0h. Three independent repeats were performed at each time point for each treatment. Error bars represent the mean ± s.d.. Data were analyzed by One-way ANOVA with Tukey's multiple-comparison test (**A, C-D**), Multiple t-tests (**A**) and Student's t test (**E-G**). Scale bar: 20 μm. $*p < 0.05$; $**p < 0.01$; $***p < 0.001$; ns, no significance. **See also in Supplementary Figure 2 and 3.**

Figure 4

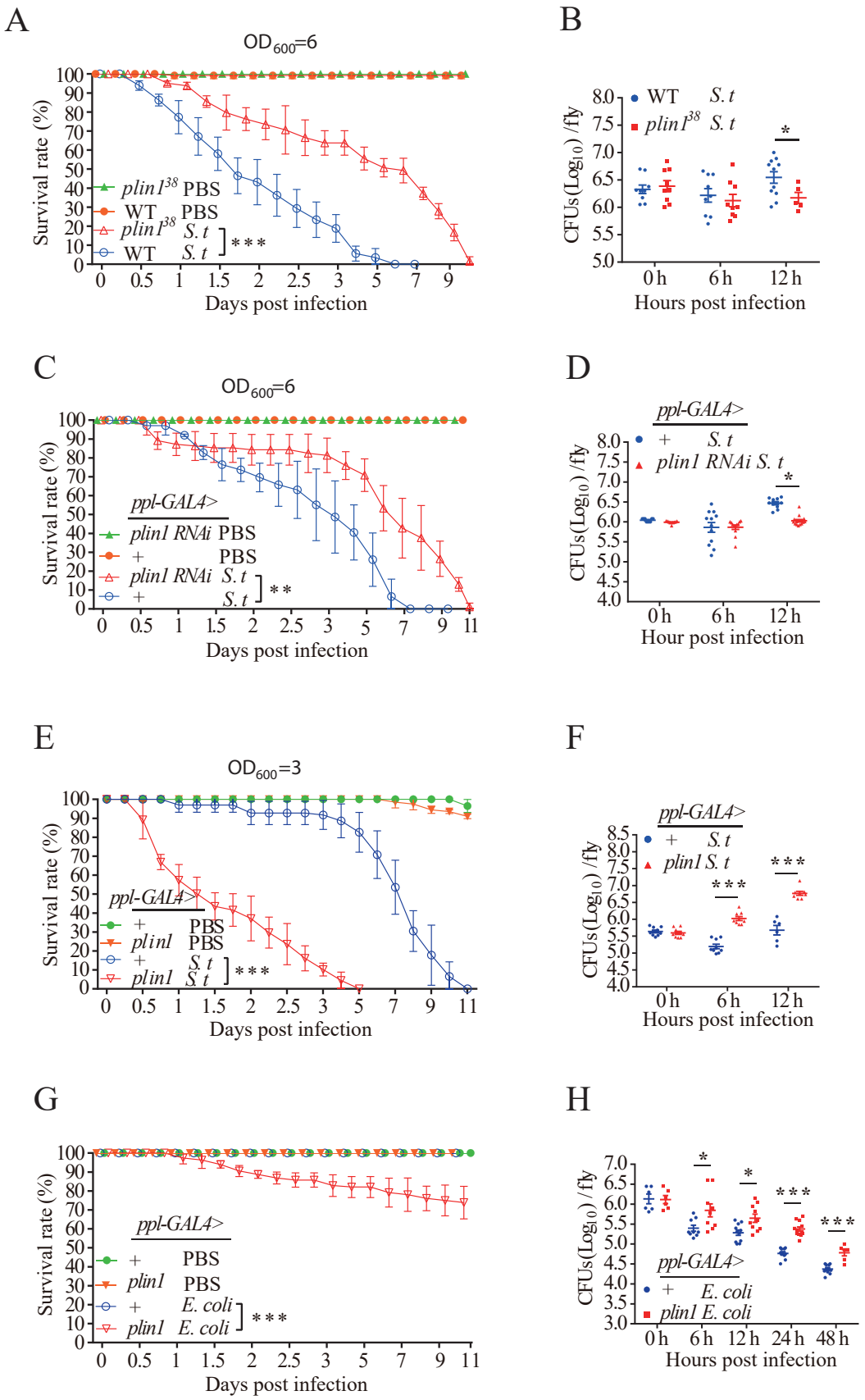
A
OD600=6
Survival rate (%)
plin1^38 PBS
WT PBS
plin1^38 S. t
WT S. t
***
Days post infection
B
WT S. t
plin1^38 S. t
CFUs(Log10) /fly
0 h
6 h
12 h
Hours post infection
C
OD600=6
ppl-GAL4>
plin1 RNAi PBS
+ PBS
plin1 RNAi S. t
+ S. t
**
Days post infection
D
ppl-GAL4>
+ S. t
plin1 RNAi S. t
Hour post infection
E
OD600=3
ppl-GAL4>
+ PBS
plin1 PBS
+ S. t
plin1 S. t
***
Days post infection
F
ppl-GAL4>
+ S. t
plin1 S. t
Hours post infection
G
ppl-GAL4>
+ PBS
plin1 PBS
+ E. coli
plin1 E. coli
***
Days post infection
H
ppl-GAL4>
+ E. coli
plin1 E. coli
24 h
48 h
Hours post infection

Fig. 4. *plin1* participates in the susceptibility of flies to bacterial infection. (**A** and **B**) Survival curves (**A**) and bacterial loads (CFUs) (**B**) of wild type and *plin1*^{38} flies (n =60) post *S. typhimurium* infection. (**C** and **D**) Survival curves (**C**) and bacterial loads (CFUs) (**D**) of *ppl-GAL4>plin1 RNAi* and control flies (n =60) post *S. typhimurium* infection. (**E** and **F**) Survival curves (**E**) and bacterial loads (CFUs) (**F**) of *ppl-GAL4>plin1* and control flies (n =60) post *S. typhimurium* infection. (**G** and **H**) Survival curves (**G**) and bacterial loads (CFUs) (**H**) of *ppl-GAL4>plin1* and control flies (n =60) post *E. coli* infection. Values of plotted curves represent mean ± s.d. (**A, C, E, G**) of at least three independent repeats. Each scattering dot (CFUs) represents one technical replicate, line represents the mean of four independent repeats (**B, D, F, H**). Data were analyzed by Kaplan–Meier (**A, C, E, G**) and Multiple t-tests (**B, D, F, H**). *$p < 0.05$; ** $p < 0.01$; *** $p < 0.001$, ns, no significance. **See also in Supplementary Figure 4.**

Figure 5

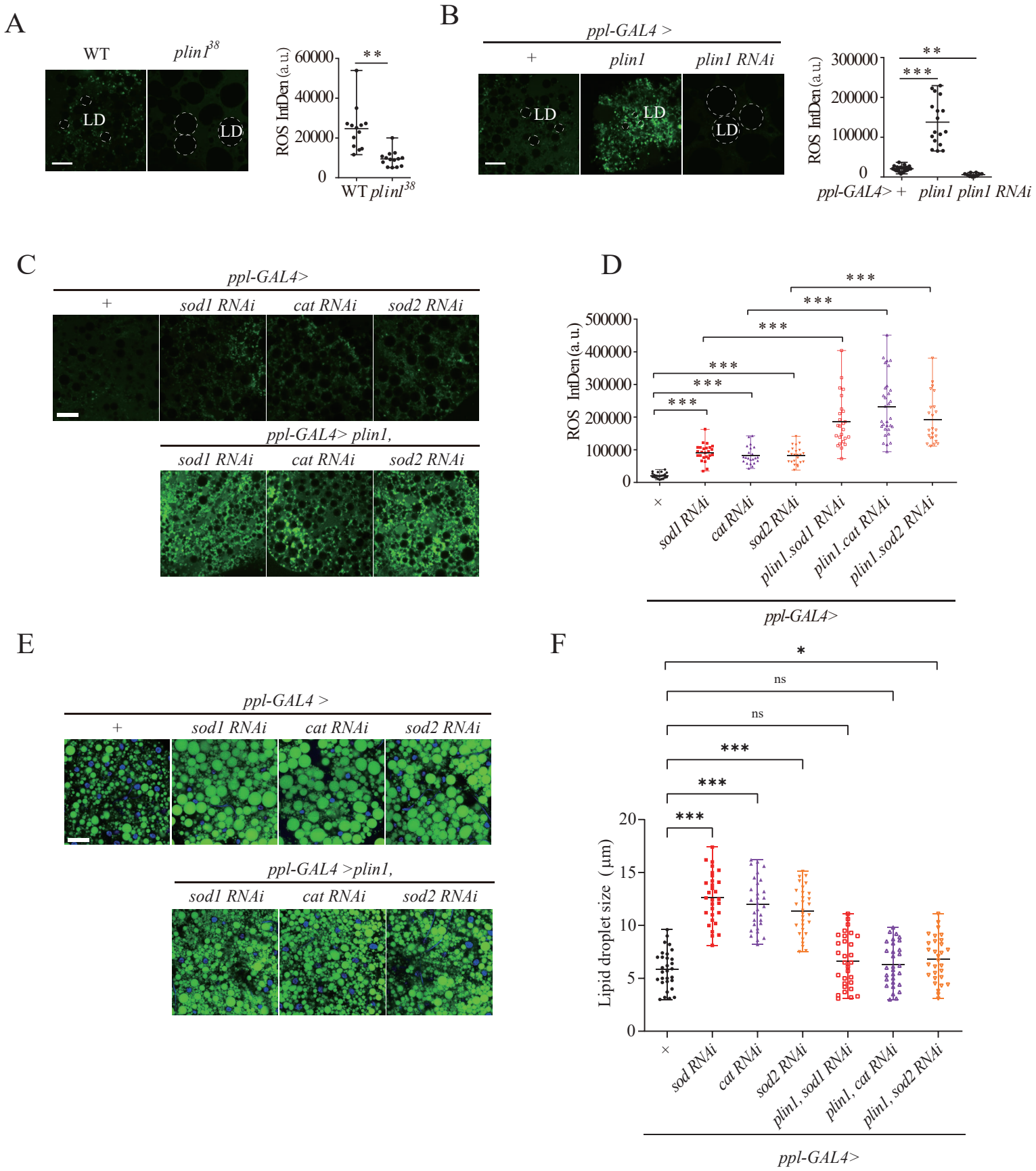
A
WT
plin1^38
LD
LD
ROS IntDen (a.u.)
60000
40000
20000
0
**
WT
plin1^38
B
ppl-GAL4 >
+
plin1
plin1 RNAi
LD
LD
LD
ROS IntDen (a.u.)
300000
200000
100000
0
**
***
ppl-GAL4> +
plin1
plin1 RNAi
C
ppl-GAL4>
+
sod1 RNAi
cat RNAi
sod2 RNAi
ppl-GAL4> plin1,
sod1 RNAi
cat RNAi
sod2 RNAi
D
ROS IntDen (a.u.)
500000
400000
300000
200000
100000
0
***
×
sod1 RNAi
cat RNAi
sod2 RNAi
plin1.sod1 RNAi
plin1.cat RNAi
plin1.sod2 RNAi
ppl-GAL4>
E
ppl-GAL4 >
+
sod1 RNAi
cat RNAi
sod2 RNAi
ppl-GAL4 >plin1,
sod1 RNAi
cat RNAi
sod2 RNAi
F
Lipid droplet size (μm)
20
15
10
5
0
*
ns
ns
***
×
sod RNAi
cat RNAi
sod2 RNAi
plin1, sod1 RNAi
plin1, cat RNAi
plin1, sod2 RNAi
ppl-GAL4>

Fig. 5. Plin1-mediated reconfiguration of LDs is involved in the regulation of intracellular ROS. (**A** and **B**) ROS level indicated by DCFH-DA staining (green) in the fat body of indicated flies. The statistics of fluorescence intensity was plotted in (**A**) for *plin1*^{38} and in (**B**) for *ppl-GAL4>plin1* and *ppl-GAL4>plin1-RNAi* flies and their genetic controls, respectively. Dashed circle indicated LDs. Eight fat bodies were examined for each sample and each scattering dot represents the data from one image. (**C** and **D**) ROS levels indicated by DCFH-DA staining (green) in the fat body of indicated one-week old adult flies and control flies (**C**). The corresponding fluorescence intensity was quantified in (**D**). Eight fat bodies were examined for each sample and each scattering dot represents the data from one image. (**E** and **F**) BODIPY staining (green) of LDs (**E**) and the corresponding statistics of LDs' size (n =30 cells) (**F**) in the fat body of indicated flies. Eight fat bodies were examined for each sample. Error bars represent the mean with range. Data was analyzed by Student's t test (**A-B, D, F**) and One-way ANOVA with Tukey's multiple comparison test (**D, F**). Scale bar: 20 μm.*$p < 0.05$; ** $p < 0.01$; *** $p < 0.001$, ns, no significance.

Figure 6

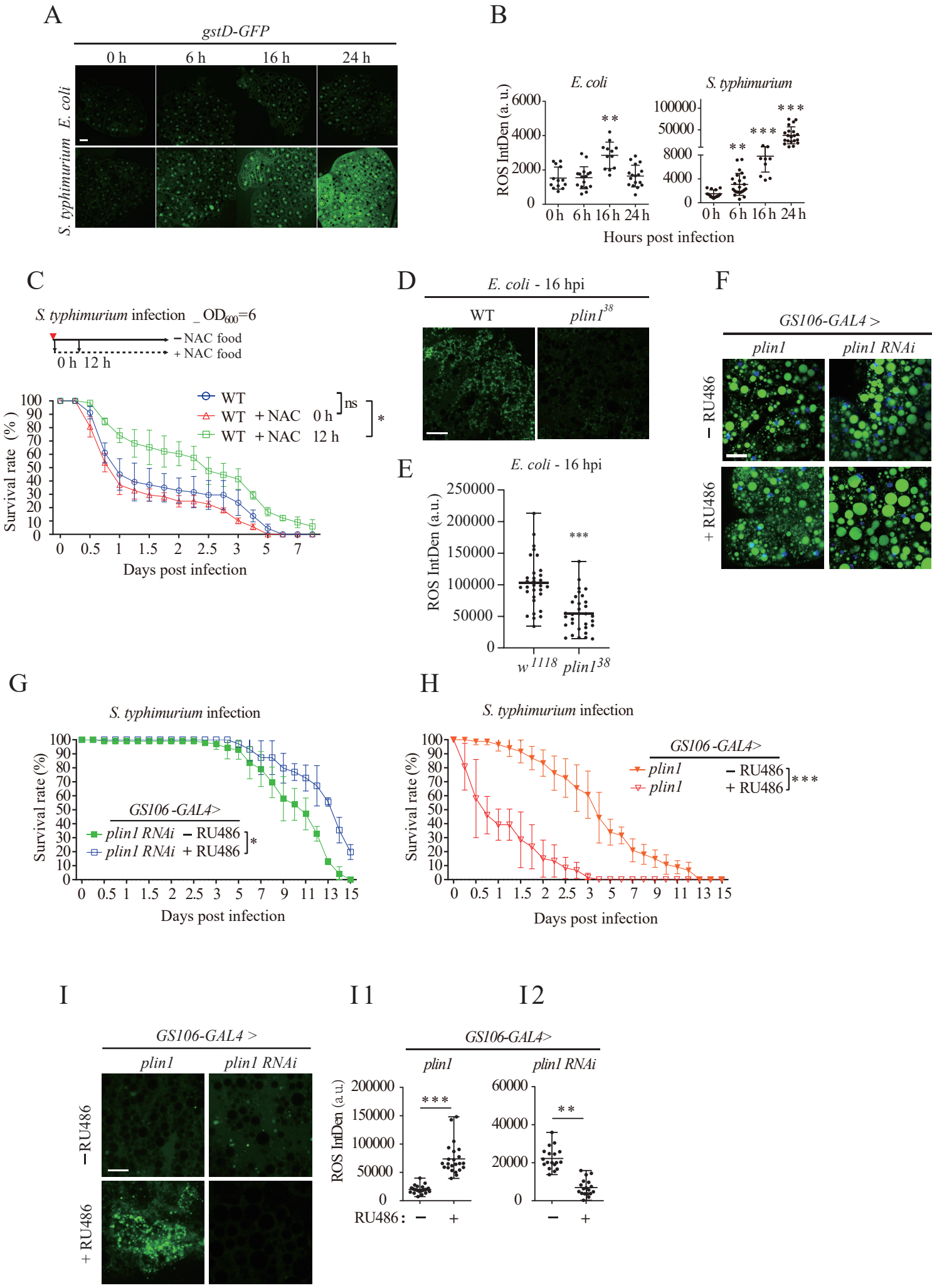
A
gstD-GFP
0 h
6 h
16 h
24 h
E. coli
S. typhimurium
B
E. coli
S. typhimurium
ROS IntDen (a. u.)
Hours post infection
C
S. typhimurium infection _ OD600=6
– NAC food
+ NAC food
0 h 12 h
WT
WT + NAC 0 h
WT + NAC 12 h
ns
*
Survival rate (%)
Days post infection
D
E. coli - 16 hpi
WT
plin1 38
E
E. coli - 16 hpi
ROS IntDen (a.u.)
w 1118
plin1 38
F
GS106-GAL4 >
plin1
plin1 RNAi
– RU486
+ RU486
G
S. typhimurium infection
GS106 -GAL4>
plin1 RNAi – RU486
plin1 RNAi + RU486
Survival rate (%)
Days post infection
H
S. typhimurium infection
GS106 -GAL4>
plin1 – RU486
plin1 + RU486
Survival rate (%)
Days post infection
I
GS106-GAL4 >
plin1
plin1 RNAi
– RU486
+ RU486
I1
I2
GS106-GAL4>
plin1
plin1 RNAi
ROS IntDen (a.u.)
RU486 : – +

Fig. 6. Downregulated Plin1 benefits flies against bacterial infection through reducing oxidative stress. (**A** and **B**) ROS level indicated by GFP intensity (green) of *gstD-GFP* reporter in the fat body of wild type flies infected with *E. coli* (upper panel) or *S. typhimurium* (lower panel) at indicated time points. The statistics of GFP intensity was plotted in (**B**) for *E. coli* infection and *S. typhimurium* infection. Eight fat bodies were examined for each sample and each scattering dot represents the data from one image. (**C**) Survival curves of wild type flies (n=60 flies) with or without NAC treatment at indicated time post *S. typhimurium* infection. (**D** and **E**) ROS level indicated by DCFH-DA staining (green) in the fat body of indicated flies at 16 h post *E.coli* infection. (**F**) BODIPY staining (green) of LDs in the fat body of *GS106-GAL4>plin1* and *GS106-GAL4>plin1 RNAi* flies after treatment with (lower panel) or without (upper panel) RU486 treatment. Eight fat bodies were examined for each sample. (**G** and **H**) Survival curves of above flies (n =60) post *S. typhimurium* infection. (**I**) ROS level indicated by DCFH-DA staining (green) in the fat body of indicated flies with (lower panel) or without (upper panel) RU486 treatment. The statistics of fluorescence intensity was plotted in (**I1**) for *GS106-GAL4>plin1* and in (**I2**) for *GS106-GAL4>plin1 RNAi* flies. Eight fat bodies were examined for each sample and each scattering dot represents the data from one image. Error bars represent the mean with range (**B, E, I**). Values of plotted curves represent mean ± s.d. of at least three independent repeats (**C, G-H**). Data was analyzed by One-Way ANOVA with Tukey's multiple-comparison test (**B**), Student's t test (**E**, **I**) and Kaplan–Meier (**C, G-H**). Scale bar: 20 μm. $*p < 0.05$; $**p < 0.01$; $***p < 0.001$, ns, no significance.

Figure 7

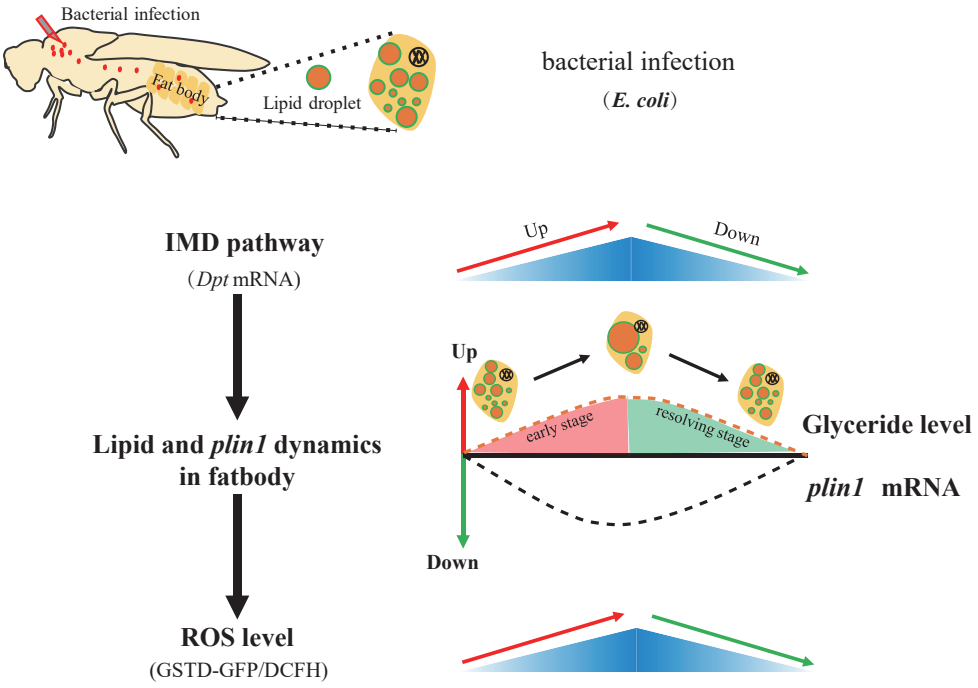
Bacterial infection
Fat body
Lipid droplet
bacterial infection
(E. coli)
IMD pathway
(Dpt mRNA)
Lipid and plin1 dynamics
in fatbody
ROS level
(GSTD-GFP/DCFH)
Up
Down
Up
early stage
resolving stage
Glyceride level
plin1 mRNA
Down

Fig. 7. The schematic diagram of LDs' morphogenesis mediated by Plin1 during infection-induced pathogenesis. LD's growth induced by downregulation of *plin1* in response to IMD signaling activation post bacterial infection. And enlarged LDs provides antioxidant role and benefits the host for anti-infection.

SUPPLEMENTAL INFORMATION

Supplemental Information includes four figures, and one table.

Supplementary Figure Legends

Figure S1

A

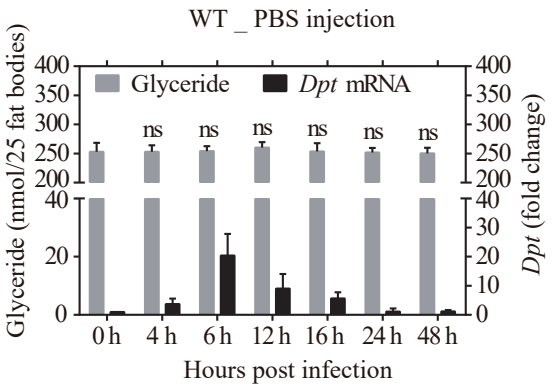
WT _ PBS injection
Glyceride
Dpt mRNA
ns
ns
ns
ns
ns
ns
Glyceride (nmol/25 fat bodies)
Dpt (fold change)
400
350
300
250
200
40
20
0
40
30
20
10
0
0 h
4 h
6 h
12 h
16 h
24 h
48 h
Hours post infection

Fig. S1. IMD signaling modifies lipid metabolism and LDs morphology. Related to Figure 1. (**A**) Relative *Dptericin* (*Dpt*) mRNA expression (black) and glyceride level (gray) in the fat body of wild type flies at indicated time points after sterile PBS injection. The fold change of mRNA expression was normalized to that of 0 h and four independent repeats (n =20 flies per repeat) were performed at each time point. Total glyceride level of 25 flies' fat body tissues was quantified in six biological replicates at each time point. Error bar mean ± s.d. Data were analyzed by One-Way ANOVA with Tukey's multiple-comparison test. $*p < 0.05$; $**p < 0.01$; $***p < 0.001$, ns, no significance.

Figure S2

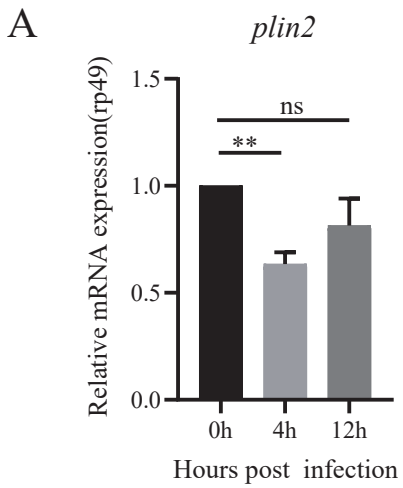
A
plin2
Relative mRNA expression(rp49)
1.5
1.0
0.5
0.0
ns
**
0h
4h
12h
Hours post infection

Fig. S2. *Plin2* expression of fat body upon *E.coli* infection. Related to Figure 3. (**A**) Relative *plin2* mRNA expression in the fat body of wild type flies at indicated time points post *E.coli* infection. The fold change of mRNA expression was normalized to that of 0 h and at least three independent repeats (n =20 flies per repeat) were performed at each time point. Error bar mean ± s.d. Data were analyzed by One-Way ANOVA with Tukey's multiple-comparison test. *$p < 0.05$; **$p < 0.01$; ***$p < 0.001$, ns, no significance.

Figure S3

A

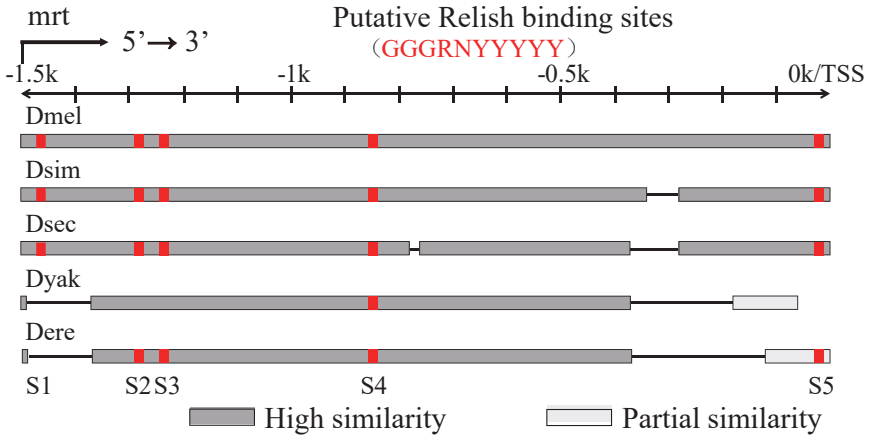

B

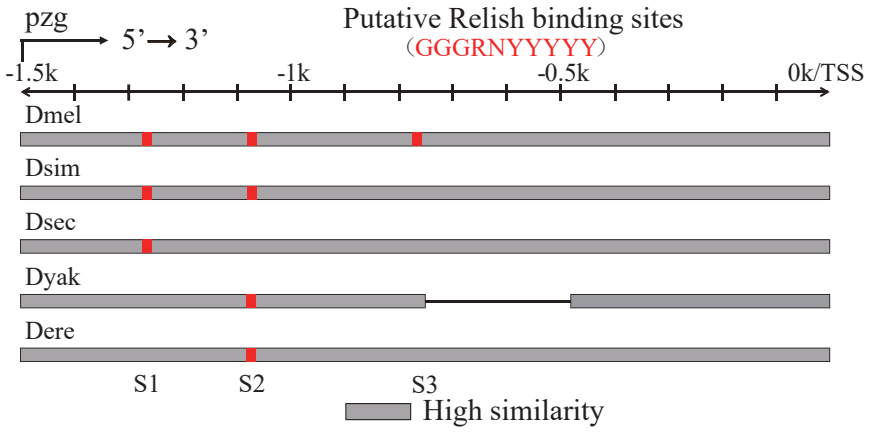

C

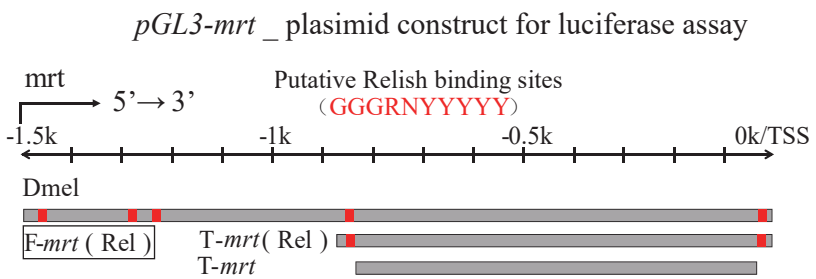

Fig. S3. Relish/NF-κB potentially regulates the transcription of *mrt* or *pzg* in *Drosophila* subgroups. Related to Figure 3. (**A and B**) Predicted Relish/NF-κB-binding motifs in the promoter locus of *mrt* (**A**) and *pzg* (**B**) genes of five *Drosophila* subgroups. Dmel, *Drosophila melanogaster*; Dsim, *D. simulans*; sec, *D. sechelia*; Dyak, *D. yakuba*; Dere, *D. erecta*. S1-S5 represent the location site (red color) of conserved binding motifs of Relish. Sequence alignment is analyzed by BLAST in flybase website. TSS: transcription start site. (**C**) Schematic diagram of the *mrt* promoter locus and the plasmid constructs used for luciferase assay. The full length (*mrt*:-1.5k to +1bp), truncated length (T-*mrt* (Rel):-870 to +1bp) and mutant length (T-*mrt*:-870 to +1bp without binding motifs) of *mrt* promoter were indicated.

Figure S4

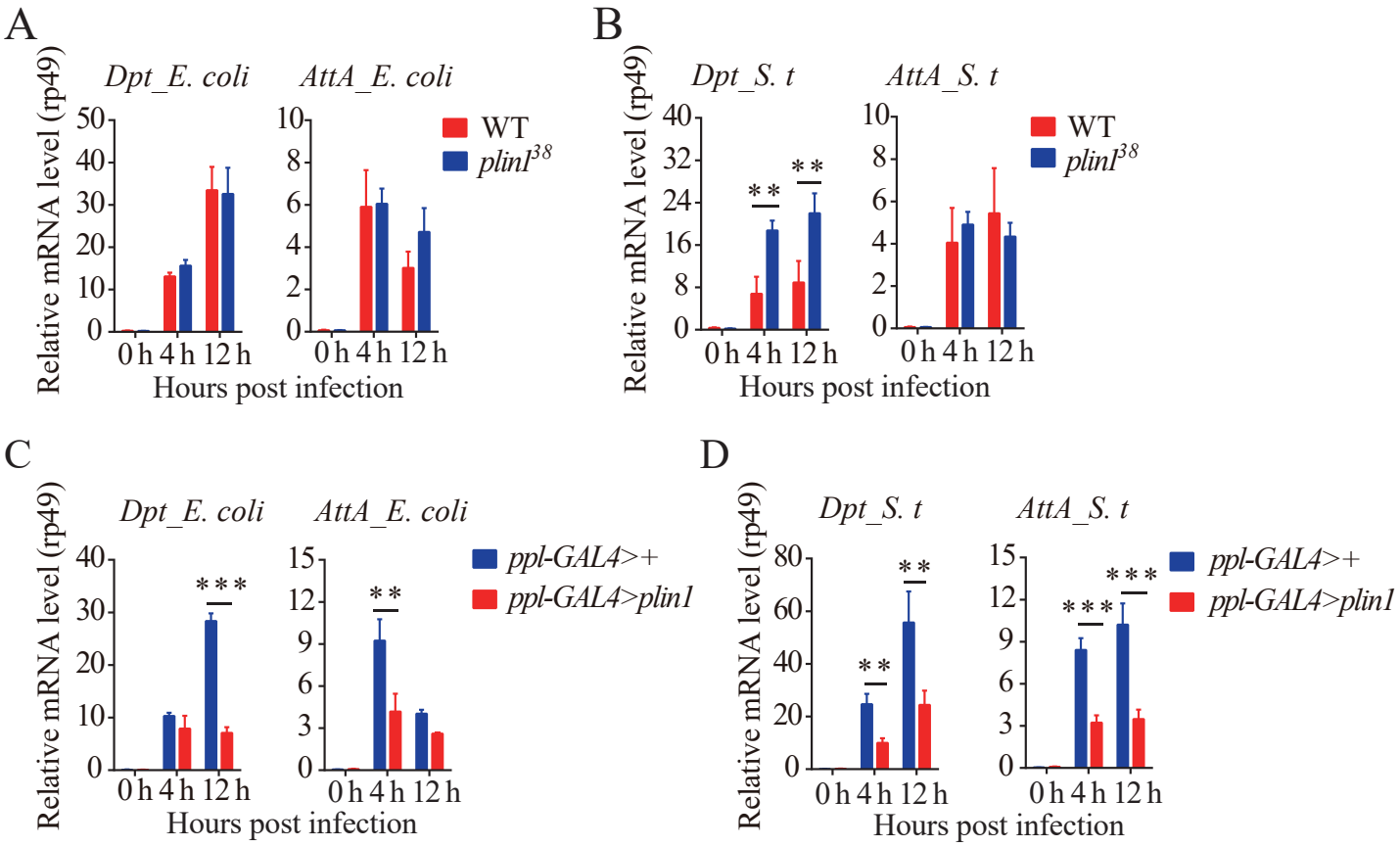
A
Dpt_E. coli
AttA_E. coli
Relative mRNA level (rp49)
WT
plinl38
0 h 4 h 12 h
Hours post infection
B
Dpt_S. t
AttA_S. t
C
ppl-GAL4>+
ppl-GAL4>plin1
D

Fig. S4. Overexpression *plin1* compromises AMP responses. Related to Figure 4. (**A** and **B**) Relative *diptericin (Dpt)* and *attacin-A (AttA)* mRNA expression in the fat body of *plin1*[38] mutant flies and wild type flies at indicated time points post *E. coli* (**A**) or *S. typhimurium* (**B**) infection. Four independent repeats were performed (n = 20 per repeat). (**C** and **D**) Relative *diptericin (Dpt)* and *attacin-A (AttA)* mRNA expression of *ppl-GAL4> plin1* flies and *ppl-GAL4>* + control flies at indicated time points post *E. coli* (**C**) and *S. typhimurium* (**D**) infection. Four independent repeats were performed (n = 20 per repeat). Error bars represent mean ± s.d. Data was analyzed by Multiple t-tests. $^{**}p < 0.01$; $^{***}p < 0.001$.

Table S1: Primers used in this study.

Genes	Forward primer	Reverse primer
	qRT-PCR primers	
Rp49	AGATCGTGAAGAAGCGCACCAAG	CACCAGGAACTTCTTGAATCCGG
Dpt	GGCTTATCCGATGCCCGACG	TCTGTAGGTGTAGGTGCTTCCC
AttA	CACAACTGGCGGAACTTTGG	AAACATCCTTCACTCCGGGC
plin1	CAGCGCATACCACTGGTCTAT	GCATTACCGATTTGCTTGACAG
plin2	CGAGCGCCTCCTTGAATAC	AGAACTCTTGCCATTCTGCAC
mrt	GGAGGATATTCTCGGAGTGGAGC	GCTTCCTGCCTCGTAGTCGAAC
pzg	GCTGAGGAACCACAACCATCTGAC	GTAACCTCGCCTTCGCCAGATT
	Primers for plasmid construction and dsRNA synthesis	
F-*mrt*(Rel)-luc	CGAGATCTGCGATCTAAGTATAACG TCGTAGCGCACACGCACACC	CAGTACCGGAATGCCAAGCTGGGT GCACCCTTTGATCAAGGTCTT
pzg-luc	CGAGATCTGCGATCTAAGTACACAG TAGCAGCACAACGGAGACG	CAGTACCGGAATGCCAAGCTCTGT AGCAGTTCTCGACGGACGCGT
T-*mrt*(Rel)-luc	CGAGATCTGCGATCTAAGTAGCCAC TTTGTCGCAGTGTATCTGT	CAACAGTACCGGAATGCCAGCTGG GTGCACCCTTTGATCAAG
T-*mrt*-luc	CGAGATCTGCGATCTAAGTACGTTA GCTTTTTGCTGTCATTCGT	CCAACAGTACCGGAATGCCAGATG CTGTTGGAAAACAAGCAA
dsRelish	TAATACGACTCACTATAGGGAGATC AAACACGTGCCGC	TAATACGACTCACTATACCCAGACT CACGCTCTGTCTC
dsGFP	TAATACGACTCACTATAGGGAGAAT GGTGAGCAAGGGCGAGGA	TAATACGACTCACTATAGGGAGACT TGTACAGCTCGTCCATGC